

(2)
EPA

Application of Satellite Accelerometer Data to Improve Density Models

FRANK A. MARCOS

AD-A154 904



9 August 1984



Approved for public release; distribution unlimited.

DTIC FILE COPY



DTIC
ELECTE
JUN 12 1985
S D
G



ATMOSPHERIC SCIENCES DIVISION

PROJECT 6690

AIR FORCE GEOPHYSICS LABORATORY

HANSCOM AFB, MA 01731

85 5 17 055

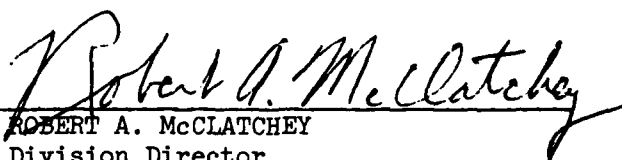
This report has been reviewed by the ESD Public Affairs Office (PA) and is releasable to the National Technical Information Service (NTIS).

"This technical report has been reviewed and is approved for publication"

FOR THE COMMANDER



DONALD D. GRANTHAM
Branch Chief



ROBERT A. McCLATCHEY
Division Director

Qualified requestors may obtain additional copies from the Defense Technical Information Center. All others should apply to the National Technical Information Service.

If your address has changed, or if you wish to be removed from the mailing list, or if the addressee is no longer employed by your organization, please notify AFGL/DAA, Hanscom AFB, MA 01731. This will assist us in maintaining a current mailing list.

Do not return copies of this report unless contractual obligations or notices on a specific document requires that it be returned.

Unclassified

SECURITY CLASSIFICATION OF THIS PAGE

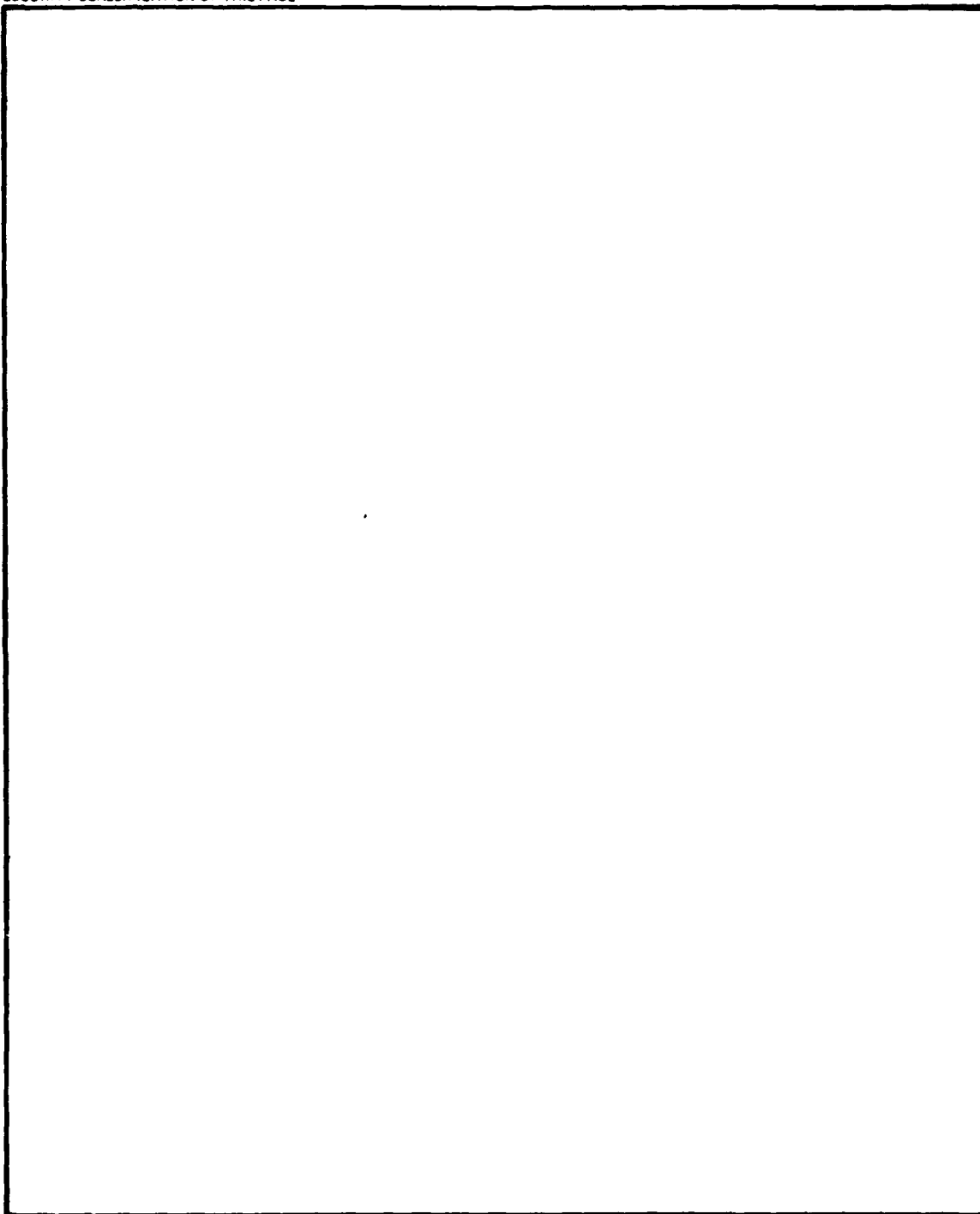
REPORT DOCUMENTATION PAGE				
1a. REPORT SECURITY CLASSIFICATION Unclassified		1b. RESTRICTIVE MARKINGS		
2a. SECURITY CLASSIFICATION AUTHORITY		3. DISTRIBUTION/AVAILABILITY OF REPORT Approved for public release; distribution unlimited.		
2b. DECLASSIFICATION/DOWNGRADING SCHEDULE				
4. PERFORMING ORGANIZATION REPORT NUMBER(S) AFGL-TR-84-0211 ERP, No. 887		5. MONITORING ORGANIZATION REPORT NUMBER(S)		
6a. NAME OF PERFORMING ORGANIZATION Air Force Geophysics Laboratory	6b. OFFICE SYMBOL (If applicable) LYT	7a. NAME OF MONITORING ORGANIZATION		
6c. ADDRESS (City, State and ZIP Code) Hanscom AFB Massachusetts 01731		7b. ADDRESS (City, State and ZIP Code)		
8a. NAME OF FUNDING/SPONSORING ORGANIZATION	8b. OFFICE SYMBOL (If applicable)	9. PROCUREMENT INSTRUMENT IDENTIFICATION NUMBER		
8c. ADDRESS (City, State and ZIP Code)		10. SOURCE OF FUNDING NOS.		
		PROGRAM ELEMENT NO. 62101F	PROJECT NO. 6690	TASK NO. 08 WORK UNIT NO. 03
11. TITLE (Include Security Classification) Application of Satellite Accelerometer Data to Improve Density Models				
12. PERSONAL AUTHOR(S) Frank A. Marcos				
13a. TYPE OF REPORT Scientific, Interim.		13b. TIME COVERED FROM _____ TO _____		14. DATE OF REPORT (Yr., Mo., Day) 1984 August 9
15. PAGE COUNT 49				
16. SUPPLEMENTARY NOTATION				
17. COSATI CODES				
FIELD	GROUP	SUB. GR.		
04	01			
22	03			
18. SUBJECT TERMS (Continue on reverse if necessary and identify by block number) Satellite, Thermospheric model evaluations, Accelerometers, Thermospheric density variability, Atmospheric density measurements.				
19. ABSTRACT (Continue on reverse if necessary and identify by block number) Atmospheric density measurements obtained by the satellite accelerometer experiment provide data over a wide range of solar and geophysical conditions. These results are used in a preliminary evaluation of several atmospheric models. The model accuracies are compared by their mean values and standard deviations relative to the accelerometer data. Sources of model uncertainties and problems in reducing them are described. Long-term programs involving coordinated measurements, analyses of available data and theoretical studies are required along with development of more accurate indicators of solar and geomagnetic activity before models can show significant improvement.				
20. DISTRIBUTION/AVAILABILITY OF ABSTRACT UNCLASSIFIED/UNLIMITED <input checked="" type="checkbox"/> SAME AS RPT <input checked="" type="checkbox"/> DTIC USERS <input type="checkbox"/>		21. ABSTRACT SECURITY CLASSIFICATION Unclassified		
22a. NAME OF RESPONSIBLE INDIVIDUAL Frank A. Marcos		22b. TELEPHONE NUMBER (Include Area Code) (617) 861-3037		22c. OFFICE SYMBOL LYT

DD FORM 1473, 83 APR

EDITION OF 1 JAN 73 IS OBSOLETE

Unclassified
SECURITY CLASSIFICATION OF THIS PAGE

SECURITY CLASSIFICATION OF THIS PAGE



SECURITY CLASSIFICATION OF THIS PAGE

Accession For	
NTIS GRA&I	<input checked="" type="checkbox"/>
DTIC TAB	<input type="checkbox"/>
Unannounced	<input type="checkbox"/>
Justification	
By	
Distribution/	
Availability Codes	
Dist	Avail and/or
A/1	Special



Contents

1. INTRODUCTION	7
2. DATA DESCRIPTION	8
3. RESULTS	15
3.1 Group I Data Mean Ratios and Standard Deviations	15
3.1.1 Frequency and Probability Distributions	18
3.1.2 Modification of Group I Data Base	18
3.1.3 Effect of Digital Filtering on Group I Data	22
3.2 Group II Data Mean Ratios and Standard Deviations	22
3.3 Data Partitioning into Kp Bins	24
3.3.1 Group I Data	24
3.3.2 Group II Data	26
3.4 Data Partitioning in Kp, Latitude and Local Time Bins	26
3.5 Effect of Digital Filtering on Group II Data	30
4. ATMOSPHERIC VARIABILITY	33
5. RECOMMENDATIONS	40
5.1 Absolute Density Determination	41
5.2 Measurements Programs	42
5.3 Supporting Studies	43
6. CONCLUSIONS	44
REFERENCES	47

Illustrations

1a.	Histogram of Group I Data Distribution as a Function of Altitude	9
1b.	Histogram of Group I Data Distribution as a Function of Solar Flux	9
1c.	Histogram of Group I Data Distribution as a Function of Geomagnetic Activity	10
1d.	Histogram of Group I Data Distribution as a Function of Local Time	10
1e.	Distribution of Group I Data at 200 km in Geographic Latitude vs Day of Year Coordinates	10
2.	Histogram of Group II Data Distribution as a Function of Solar Flux	11
3.	Histogram of Group II Data Distribution as a Function of Geomagnetic Activity	12
4.	Solar Flux and Geomagnetic Activity Indicators vs Day of Year for SETA-2 Data	12
5.	Distribution of Group II Data in Geographic Latitude vs Day of Year Coordinates	13
6.	Satellite Accelerometer Density Data Sources Utilized for Statistical Analyses	14
7a.	Density Variation at 160 km as a Function of Local Time (Day = 81, Latitude = 0°, F = F _{min} = 75, Kp = 0)	17
7b.	Density Variation at 200 km as a Function of Local Time (Day = 81, Latitude = 0°, F = F _{min} = 75, Kp = 0)	17
7c.	Density Variation at 240 km as a Function of Local Time (Day = 81, Latitude = 0°, F = F _{min} = 75, Kp = 0)	18
8a.	Frequency Distribution of Percent Difference of AE-C Data From J71 Model	19
8b.	Frequency Distribution of Percent Difference of AE-D Data From J71 Model	20
9a.	Probability Distributions for AE-C Data Shown as Percent Departure From the J71 Model	20
9b.	Probability Distributions for AE-D Data Shown as Percent Departure From the J71 Model	21
10.	Mean Values of Ratios of SETA-1, SETA-2 and S3-4 Density Data to J71 Model Plotted as a Function of Geographic Latitude (Kp ≤ 3)	28
11a.	Standard Deviations of Ratios of SETA-1 Density Data to J71 Model Plotted as a Function of Geographic Latitude	29
11b.	Standard Deviations of Ratios of SETA-2 Density Data to J71 Model Plotted as a Function of Geographic Latitude	30
11c.	Standard Deviations of Ratios of S3-4 Density Data to J71 Model Plotted as a Function of Geographic Latitude	31
12.	Standard Deviations of Ratios of S3-1 Density Data to J71 Model Plotted as a Function of Geographic Latitude	32
13.	Effect of Digital Filter Bandwidth on SETA-2 Standard Deviations for (a) MSIS77 Model and (b) J71 Model for Quiet Geomagnetic Conditions	33

Illustrations

14. Standard Deviations of Ratios of SETA-2 Data to MSIS77 Model for Low, Moderate and High Geomagnetic Periods Plotted as a Function of Geographic Latitude	34
15. Schematic Representation of Heat Sources for the Upper Atmosphere	35

Tables

1. Satellite Accelerometer Data Sources	8
2. Group I (AE-C, -D, -E and S3-1) Total Mass Density Ratio to Models (Altitude = 135-240 km; Local Time = 0-24 hr; Kp Range = 0-9)	16
3. Modified Group I (AE-C, -D and -E) Total Mass Density Ratio to Models (Altitude = 170-220 km; Local Time = 08-24 hr; Kp Range = 0-9)	21
4. Comparison of Modified Group I (AE-C, -D and -E) Spun and Despun Mode Total Mass Density Ratio to Models (Altitude = 170-220 km; Local Time = 08-24 hr; Kp Range = 0-9)	22
5. Group II (SETA-1, SETA-2 and S3-4) Total Mass Density Ratio to Models (Altitude = 170-220 km; Local Time = 08-24 hr; Kp = 0-9)	23
6. Modified Group I (AE-C, -D and -E) Spun and Despun Mode Total Mass Density Ratio to Models Partitioned into Kp Bins	25
7. Group II (SETA-1, SETA-2, and S3-4) Total Mass Density Ratio to Models Partitioned into Kp Bins	27
8. Thermospheric Density Variability at 200 km	40

Application of Satellite Accelerometer Data to Improve Density Models

1. INTRODUCTION

AFGL is obtaining comprehensive solar-cycle coverage of atmospheric density variations in the lower thermosphere (between about 140 and 240 km) from satellite accelerometer measurements. We accumulated extensive low solar flux data during 1974 - 1976 from the S3-1 and Atmosphere Explorer -C, -D and -E (AE-C, -D, -E) experiments.¹ This data set has been incorporated into an empirical model of density variability during low solar flux conditions.² Results for moderate to high solar activity periods are becoming available from the ROCA³ and SETA⁴ (SETA-1 and -2) instruments. Although only samples of these data are available for analysis, our accelerometer density data base is being continually expanded as new results

(Received for publication 8 August 1984)

1. Marcos, F. A., McInerney, R. E., and Floretti, R. W. (1978) Variability of the Lower Thermosphere Determined From Satellite Accelerometer Data, AFGL-TR-78-0134, AD A058982.
2. Marcos, F. A., Gillette, D. F., and Robinson, E. C. (1982) A Global Thermospheric Density Model Based on Satellite Accelerometer Data, AFGL-TR-82-0025, AD A119861.
3. Marcos, F. A., and Champion, K. S. W. (1979) Satellite Density Measurements With a Rotatable Calibration Accelerometer (ROCA), AFGL-TR-79-0005, AD A069740.
4. Marcos, F. A., and Swift, E. R. (1982) Application of the Satellite Triaxial Accelerometer to Atmospheric Density and Wind Studies, AFGL-TR-82-0091, AD A120852.

become available. This data base permits systematic analyses of atmospheric density variability and eventual development of improved models.

A statistical evaluation of several atmospheric models using selected data from SETA-1, SETA-2, and ROCA has been compared with similar analyses using the low solar flux data from S3-1 and AE-C, -D, and -E. Our present knowledge of absolute density and its variations, based mainly on these results, is discussed along with a brief review of the nature of the problem and requirements for achieving improved accuracies. This preliminary assessment is in response to a Space Division need for a summary of our present and future capability to specify atmospheric density in the lower thermosphere.

2. DATA DESCRIPTION

Table 1 lists the sources of the present data set and the dates of data acquisition. The single axis MESA (Miniature Electrostatic Accelerometer),⁵ flown on AE-C, -D and -E (triaxial configuration) and on S3-1, has been described previously.^{1, 2} On the S3-4 satellite the MESA unit was mounted on a table which could be rotated perpendicular to the satellite flight direction.³ This ROCA (Rotatable Calibration Accelerometer) experiment provided an orbital bias calibration capability. The SETA (Satellite Electrostatic Triaxial Accelerometer) instruments⁴ permit simultaneous measurements of three orthogonal acceleration components with a single proof mass. Horizontal and vertical winds, as well as density, can be determined using only one instrument.

Table 1. Satellite Accelerometer Data Sources

Satellite	Data Acquisition Period
AE-C	Jan - Dec 74
S3-1	Oct 74 - May 75
AE-D	Oct 75 - Jan 76
AE-E	Nov 75 - Nov 76
S3-4	May - Aug 78
SETA-1	Mar - Apr 79
SETA-2	May - Nov 82

5. Champion, K.S.W., and Marcos, F.A. (1973) The triaxial accelerometer system on Atmosphere Explorer, Radio Sci. 8:197.

The data sets of Table 1 have been divided into two groups. Group I consists of the low solar flux data from S3-1 and AE-C, -D and -E. Group II consists of the moderate to high solar flux data from S3-4 (ROCA) and SETA-1, -2. The major features of the Group I data distribution^{1,2} summarized in Figures 1a-1e are:

- (a) Altitude coverage 135-240 km.
- (b) Low solar flux conditions, with 96 percent of the data at $F_{10.7} \leq 100$ units.
- (c) An extensive range of geomagnetic conditions.
- (d) Good local time coverage, particularly from AE-C and AE-E.

(e) Latitude coverage mainly at low and middle latitudes with 79 percent of the data between the equator and $\pm 60^\circ$ (geographic). There is a non-uniform distribution of the latitudinal coverage. High latitude data ($> 60^\circ$) occur mainly during winter and spring over the northern hemisphere and during summer over the southern hemisphere.

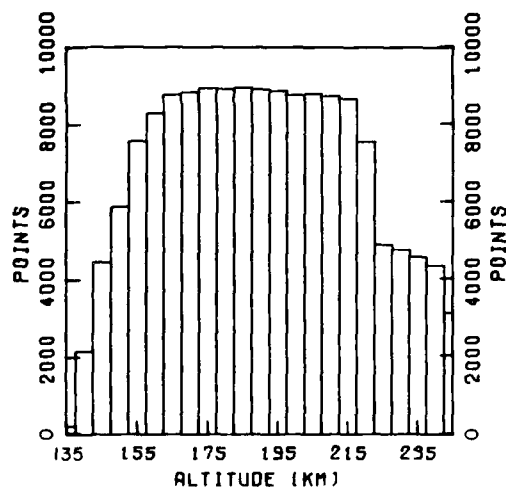


Figure 1a. Histogram of Group I Data Distribution as a Function of Altitude

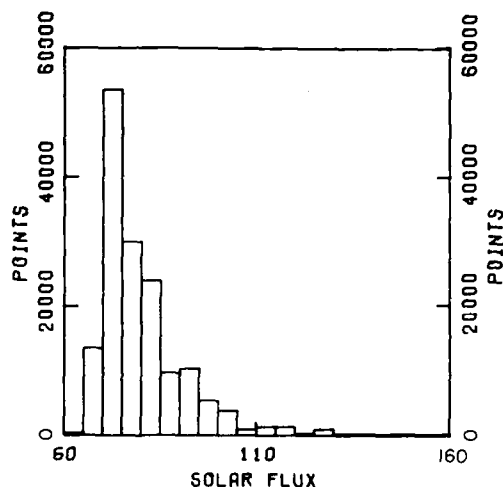


Figure 1b. Histogram of Group I Data Distribution as a Function of Solar Flux

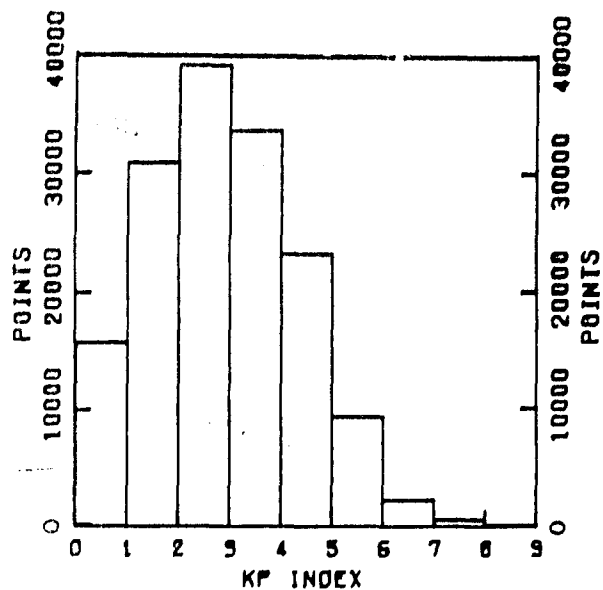


Figure 1c. Histogram of Group I Data Distribution as a Function of Geomagnetic Activity

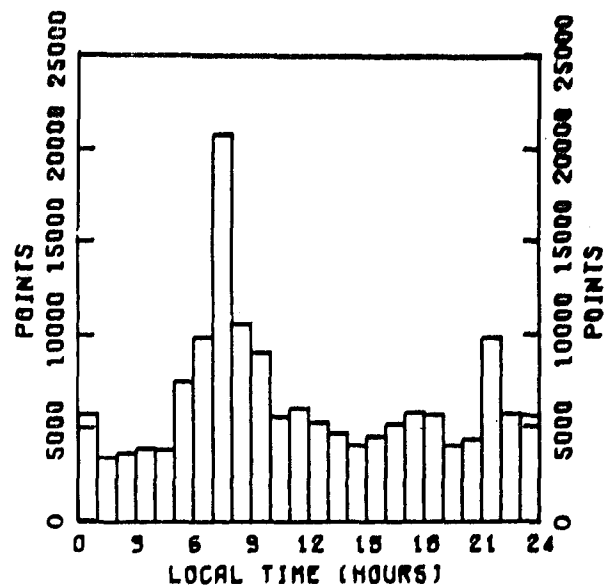


Figure 1d. Histogram of Group I Data Distribution as a Function of Local Time

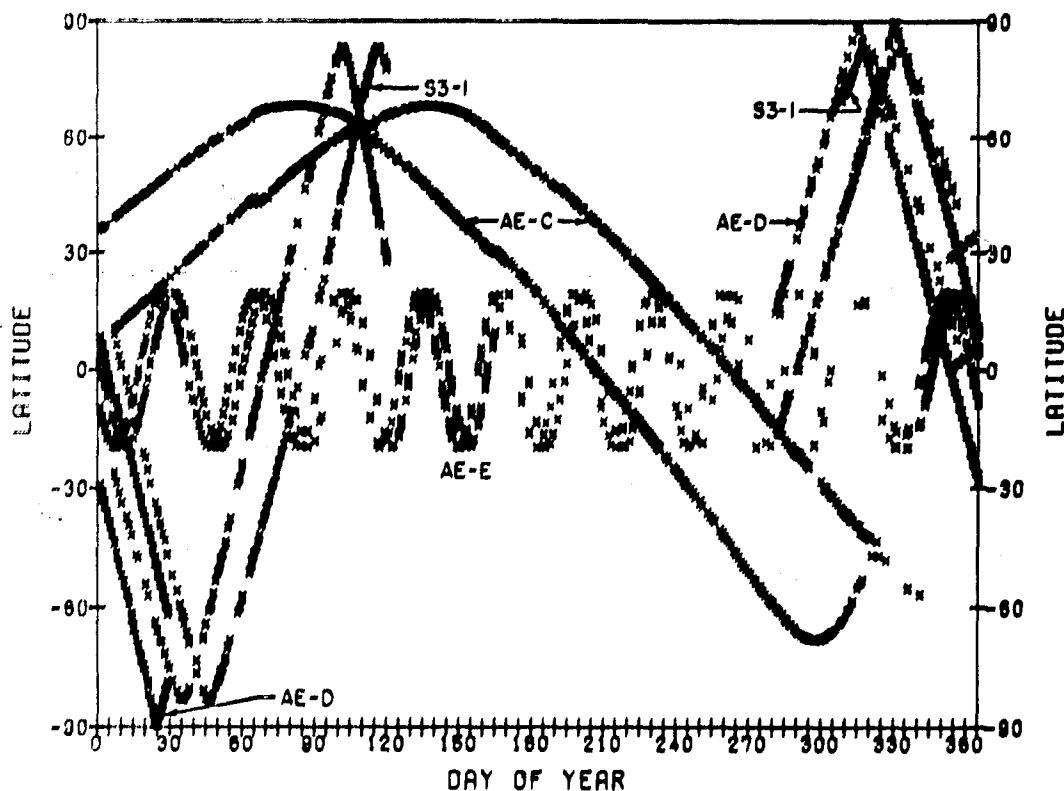


Figure 1e. Distribution of Group I Data at 200 km in Geographic Latitude vs Day of Year Coordinates

The available Group II data, obtained between 170-240 km, complement and extend the Group I data. Figure 2 shows that the solar flux conditions extend over a range of almost 200 units to a maximum value of 276 units. Therefore, the data are for moderate to high solar activity. Figure 3 is a histogram of the distribution of geomagnetic activity (Kp) showing that a wide range of conditions was encountered, very much like that for Group I (Figure 1c). Figure 4 is presented in order to summarize the dramatic variations in solar and geomagnetic conditions encountered during the SETA-2 flight. The $F_{10.7}$ cm solar flux and daily sum of the 3-hourly Kp index are shown as function of day of year, from 1 May - 7 October 1982. Distribution of the data in day of year vs geographic latitude is shown in Figure 5. Results are obtained from the northern hemisphere polar region to about 40° south latitude from March to November. The major feature of the Group II data are:

- (a) Altitude coverage approximately 170-240 km.
- (b) Moderate to high solar flux conditions.
- (c) Local times mainly near 1030 and 2230 hours.
- (d) Nearly uniform latitudinal coverage from north polar regions to about 40°S for the period March - November.

The combination of an extensive lower thermosphere density data set obtained over a wide latitude region with routine monitoring at high latitudes has not been previously achieved. The present and planned Group II data provide a unique opportunity to investigate the role of the various heat sources that affect neutral atmospheric density. For example, effects of geomagnetic storms can now be studied to determine their dependence on latitude, season and solar flux at morning and evening local times. Further, any proposed improved indicators of solar and geomagnetic activity can be readily evaluated.

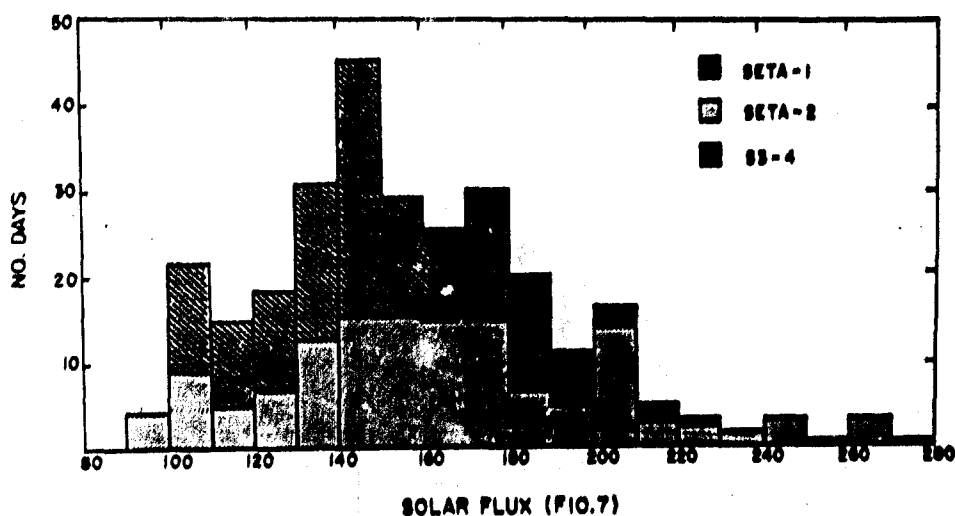


Figure 2. Histogram of Group II Data Distribution as a Function of Solar Flux

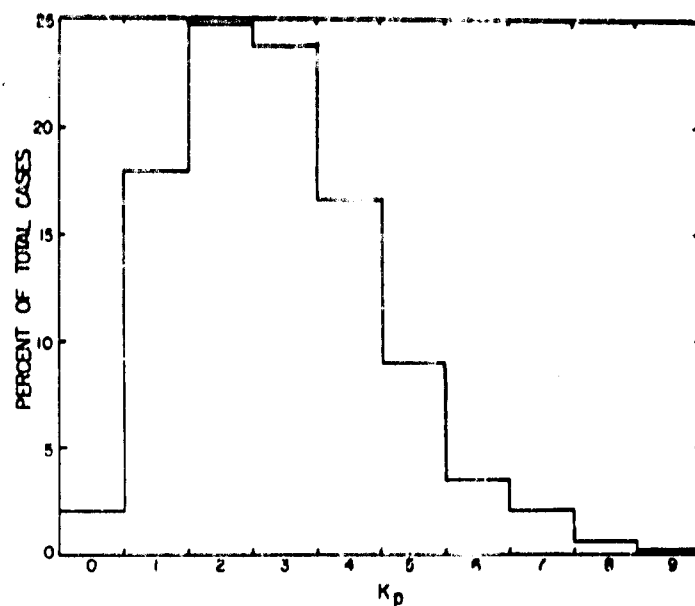


Figure 3. Histogram of Group II Data Distribution as a Function of Geomagnetic Activity

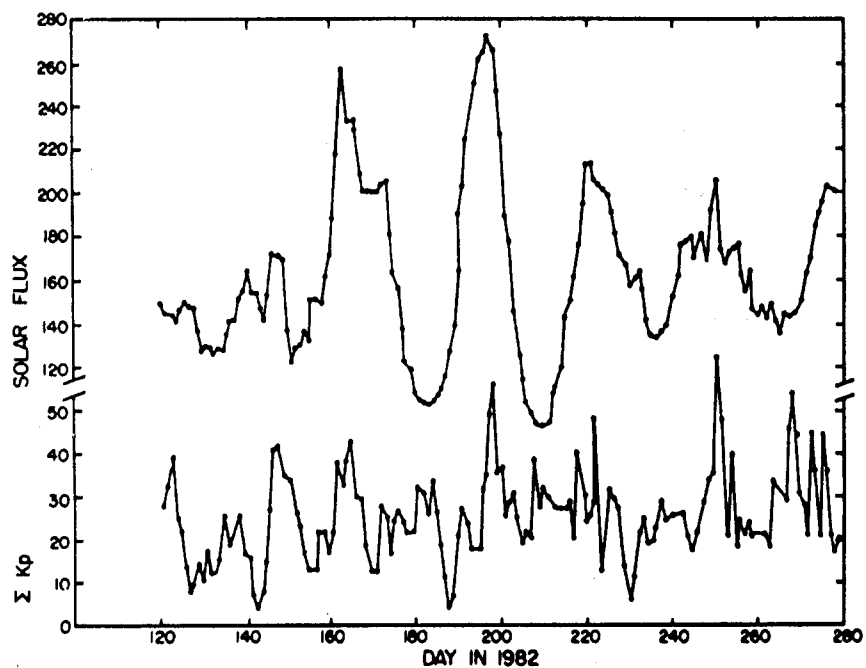


Figure 4. Solar Flux and Geomagnetic Activity Indicators vs Day of Year for SETA-2 Data

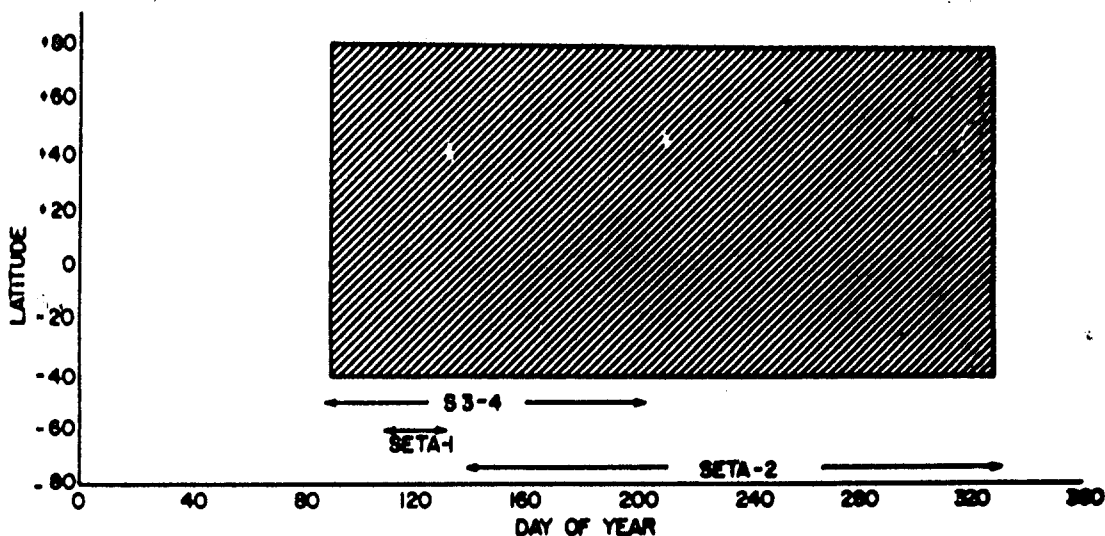


Figure 5. Distribution of Group II Data in Geographic Latitude vs Day of Year Coordinates

Figure 6 outlines the data selection and analysis performed for this study. The satellites, time periods of measurements and total number of orbits for which data are available are given in the top boxes. Portions of each data set utilized are shown in the next row. Various sub-sets were studied and are specified as required in the next section. Software was developed to calculate ratios of measured density to numerous models in the "Model Ratio Program." The models considered were six versions by Jacchia: J64, J70, J71, J73, and JWB (see Reference 6 and references therein) and J77,⁷ the MSIS (Mass Spectrometer and Incoherent Scatter) model without (MSIS77)⁸ and with (MSIS79)⁹ longitude variations, the U.S. Standard Atmosphere 1962,⁶ the U.S. Standard Atmosphere Supplements, 1966,⁶ the Lockheed-NASA model⁶ and DENSEL.⁶ The ratios were used as input to a "Statistics Program" for calculations of mean values and standard deviations in selected Kp, latitude and local time bins.

6. Bramson, A. S., and Slowey, J. W. (1974) Some Recent Innovations in Atmospheric Density Programs, IBM Corp., AFCRL-TR-74-0379, AD 786414.

7. Jacchia, L. G. (1977) Thermospheric Temperature Density and Composition: New Models, Special Report 375, Smithsonian Astrophys. Observatory, Cambridge, Massachusetts.

8. Hedin, A. E., Salah, J. E., Evans, J. V., Reber, C. A., Newton, G. P., Spencer, N. W., Kayser, D. C., Alcayde, D., Bauer, P., Cogger, L., and McClure, J. P. (1977) A global thermospheric model based on mass spectrometer and incoherent scatter data, MSIS 1, N₂ density and temperature, J. Geophys. Res. **82**:2139.

9. Hedin, A. E., Reber, C. A., Spencer, N. W., and Brinton, H. C. (1979) Global model of longitude/UT variations in thermospheric composition and temperature based on mass spectrometer data, J. Geophys. Res. **84**:1.

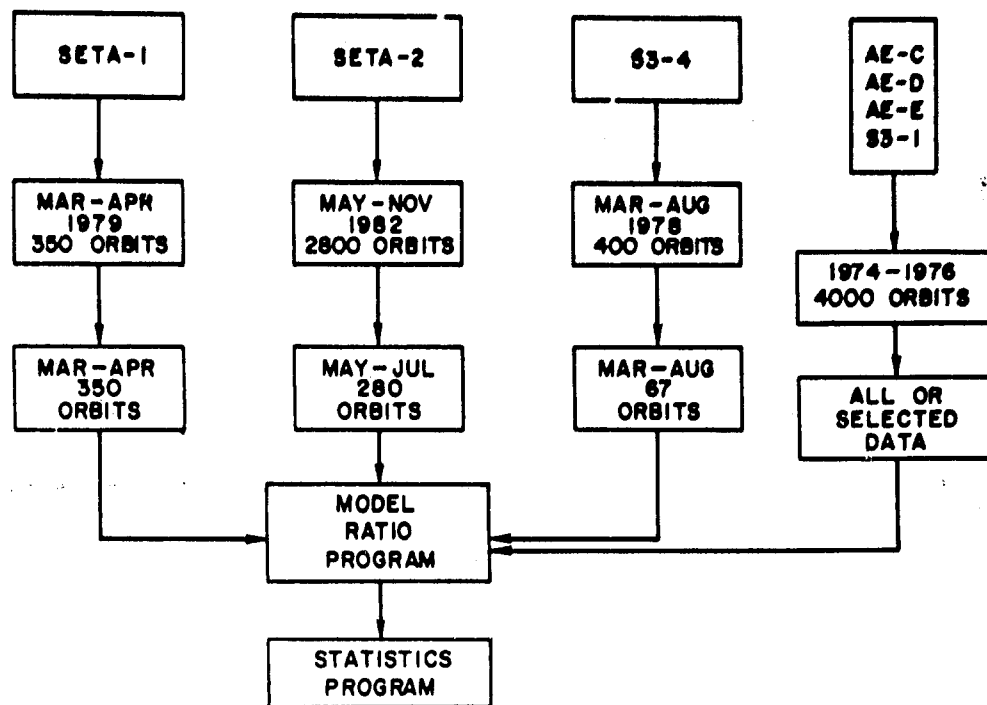


Figure 6. Satellite Accelerometer Density Data Sources Utilized for Statistical Analyses

Digital filters were used to separate drag from extraneous noise accelerations in deriving atmospheric density from accelerometer data. These filters differed, depending mainly upon the spacecraft spin rate. Comparison of standard deviations between different data sets requires consideration of the data smoothing due to the filtering. For the Atmosphere Explorer-C, -D and -E satellites, data obtained in the "despun" mode (one revolution per orbit) were reduced using a "10-15"-sec filter. This filter rejects all data with a period less than or equal to 10 sec and passes all data with a period equal to or greater than 15 seconds. Between these two values the filter "transmission coefficient" increases from zero to 100 percent with a quarter sine wave shape. Data obtained in the "spinning" mode (nominally one revolution per 15 sec) were reduced using a "30-77"-sec filter.¹⁰ Therefore, assuming a satellite velocity of 8 km/sec, atmospheric phenomena with wavelengths less than about 80 km (despun data) or 240 km (spinning data) are smoothed out by the digital filtering. Data from S3-1 were processed by first applying a "notch" filter to remove noise with periods between 13 and 50 sec, calculating density as a function of time and then applying a "4-8"-sec filter. For the Group II data a

10. Noonan, J. P., Floretti, R. W., and Hass, B. (1975) Digital Filtering Analysis Applied to the Atmosphere Explorer-C Satellite MESA Accelerometer Data, AFCRL-TR-75-0293, AD A015765.

"50-100"-sec filter was generally used. A special study of higher frequency atmospheric structure was also conducted using ten days of SETA-2 data processed with a "15-20"-sec filter.

3. RESULTS

3.1 Group I Data Mean Ratios and Standard Deviations

Table 2 provides a statistical evaluation of the entire AE-C, -D and -E and S3-1 data base. As noted in Section 2, the quantity statistically analyzed is the ratio (R) between the measured density and model density. Results are given for mean ratios (\bar{R}):

$$\bar{R} = \frac{1}{N} \sum_{n=1}^N R \quad (1)$$

and standard deviations (σ_R):

$$\sigma_R = \left[\frac{1}{N-1} \sum_{n=1}^N (R - \bar{R})^2 \right]^{1/2} \quad (2)$$

where N is the number of data points. Models used for this study are listed in order of increasing percent standard deviation. For the first three models listed, the mean ratios are within 1.045 ± 0.025 and the standard deviations are within 14.5 ± 0.3 percent, indicating excellent overall agreement. Note that the unpublished J73 model has the lowest standard deviation, 0.6 percent less than that of J71. At the other extreme, the root-mean-square (rms) variations for the DENSEL ratio are exceeded only by US62 for this low solar flux data set.

The empirical Atmospheric Density Model (ADM)² developed from the above data set has been used to evaluate other model depictions of density variability with solar flux, geomagnetic activity, local time and day of year. As an example of that analysis, Figures 7a-7c, taken from Reference 2, compare the local time dependence of density from ADM with that of the J71, J77 and MSIS77 models. At 160 km the local time behavior is dominated by the semidiurnal tide, in very good agreement with the MSIS model and contrary to the J71 and J77 diurnal tide predictions. At 200 km and 240 km the diurnal tide becomes predominant, but appears to be overestimated in J71 and J77 and underestimated in MSIS. A statistical evaluation of ADM, using the total data set it is based upon, provided the following result:

<u>Model</u>	<u>Mean Ratio</u>	<u>Std. Dev. (%)</u>
ADM	1.000	12.8

This standard deviation is 1.4 percent smaller than that of J73. The calculated standard deviation represents an internal test of the consistency between the mathematical representation and the data set used for model development. The actual test of a model is its ability to represent independent data (not used in its construction). However, preliminary tests, using a model constructed from a portion of the data and evaluating it with the remainder of the data, have indicated the improved accuracy of ADM. These tests included evaluating a model based on only northern hemisphere data with data obtained in the southern hemisphere and evaluating a model based on three satellite data sets with results from the fourth data set. Future efforts directed toward incorporating the Group II data into an improved version of the ADM model can lead to increased understanding of density variability at high latitudes and high solar flux conditions.

Table 2. Group I (AE-C, -D, -E and S3-1) Total
Mass Density Ratio to Models (Altitude = 135-240 km;
Local Time = 0-24 hr; Kp Range = 0-9)

Model	Mean Ratio	Std Dev (%)
1. J73	1.057	14.2
2. MSIS (77)	1.021	14.6
3. J71	1.070	14.8
4. J77	1.032	15.6
5. J70	1.022	15.8
6. US66	0.931	16.1
7. L-NASA	0.910	16.6
8. J64	0.921	17.3
9. JWB	1.000	19.6
10. DENSEL	1.214	28.1
11. US62	0.773	33.6

Total No. of Points = 154,749

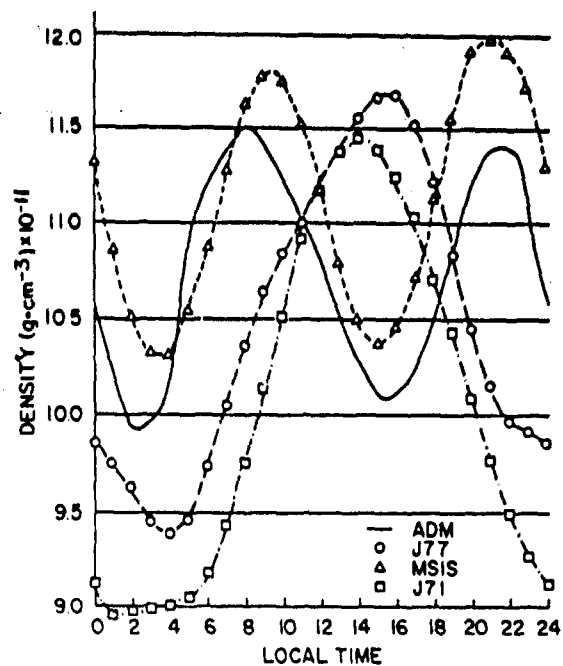


Figure 7a. Density Variation at 160 km as a Function of Local Time (Day = 81, Latitude = 0°, $F = \bar{F} = 75$, $K_p = 0$)

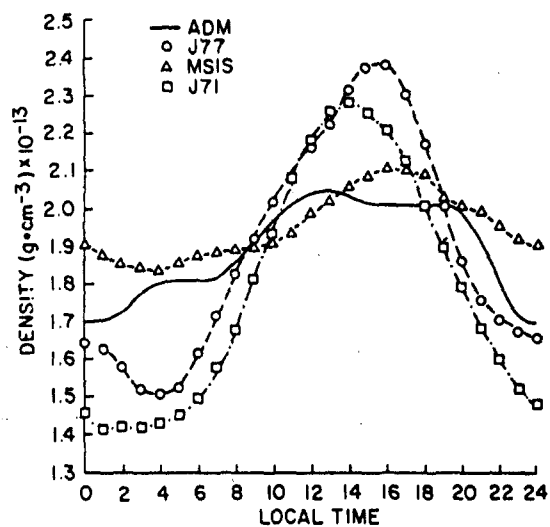


Figure 7b. Density Variation at 200 km as a Function of Local Time (Day = 81, Latitude = 0°, $F = \bar{F} = 75$, $K_p = 0$)

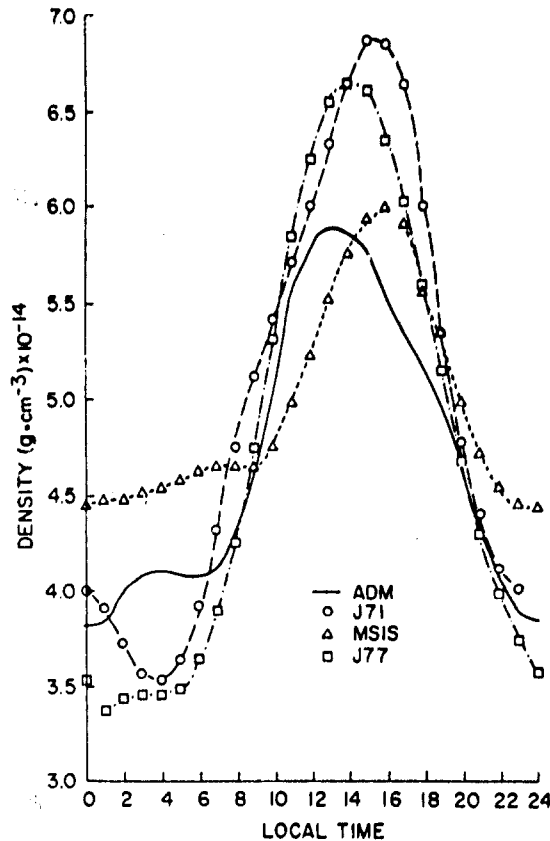


Figure 7c. Density Variation at 240 km as a Function of Local Time (Day = 81, Latitude = 0°, $F = \bar{F} = 75$, $Kp = 0$)

3.1.1 FREQUENCY AND PROBABILITY DISTRIBUTIONS

Histograms of the frequency distribution and curves of the probability distribution of the data, shown as percent departure from models were given for Group I data in Reference 1. That study included calculations of the third and fourth moments (skewness and kurtosis, respectively) as well as the mean and standard deviation. Although results showed some deviations from a normal distribution, there are no infrequently occurring very large differences. Data for AE-C and AE-D are reproduced in Figures 8a and 8b, and their cumulative probability distributions are shown in Figures 9a and 9b. Similar analyses are planned using the Group II data.

3.1.2 MODIFICATION OF GROUP I DATA BASE

The Group I data base was modified by considering only Atmosphere Explorer data and limiting results to the region 170-220 km for local times 08-24 hr. This was done to provide a data set that was more self-consistent and more compatible for later comparison with the Group II data. The AE satellites had similar orbital parameters, shapes, drag coefficients and error sources. Density values were derived with identical filters. The 170-220 km region is also used for the Group II

data for this report and all Group II data points have local times between 08 and 24 hr, although they are heavily concentrated near 10 and 22 hrs (limiting the Atmosphere Explorer data base to a similar local time distribution would result in elimination of about 90 percent of the available data). Statistical results given in Table 3 for this limited Group I data set show MSIS77 has the smallest standard deviation, 1 percent less than its value for all data (Table 2). For the first three models of Table 3 the standard deviations are reduced to 13.9 ± 0.3 percent. Thus, the restricted altitude and local time range results in a reduction of at least 0.6 percent in the standard deviation.

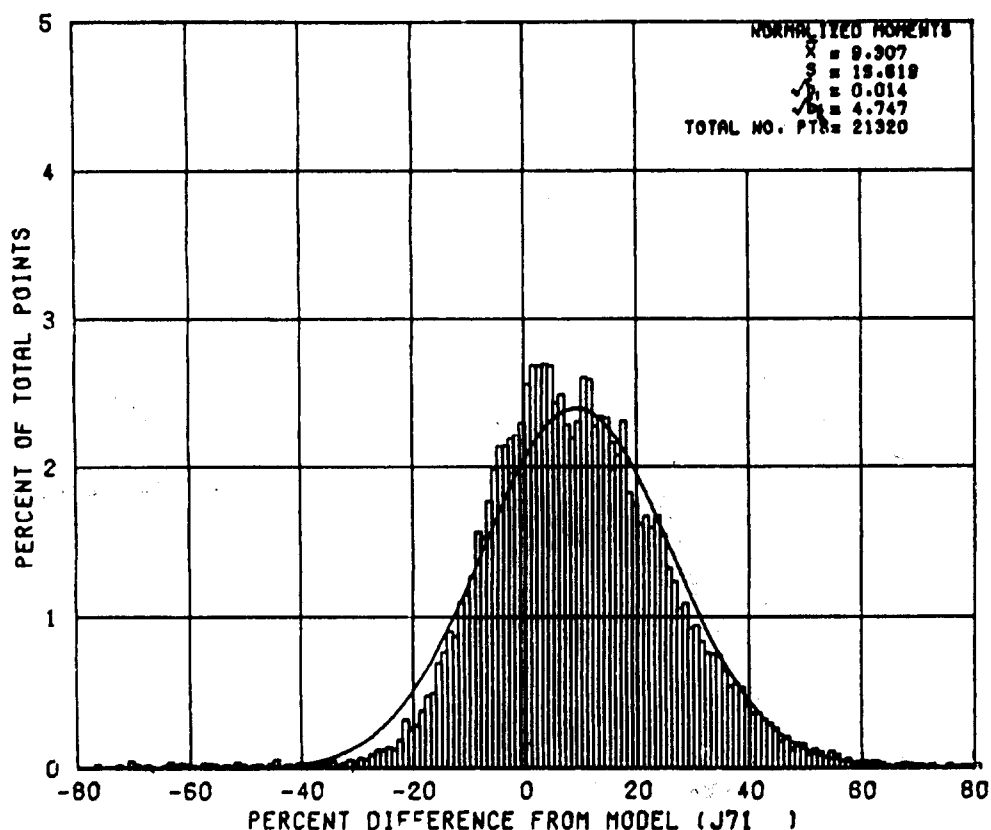


Figure 8a. Frequency Distribution of Percent Difference of AE-C Data From J71 Model

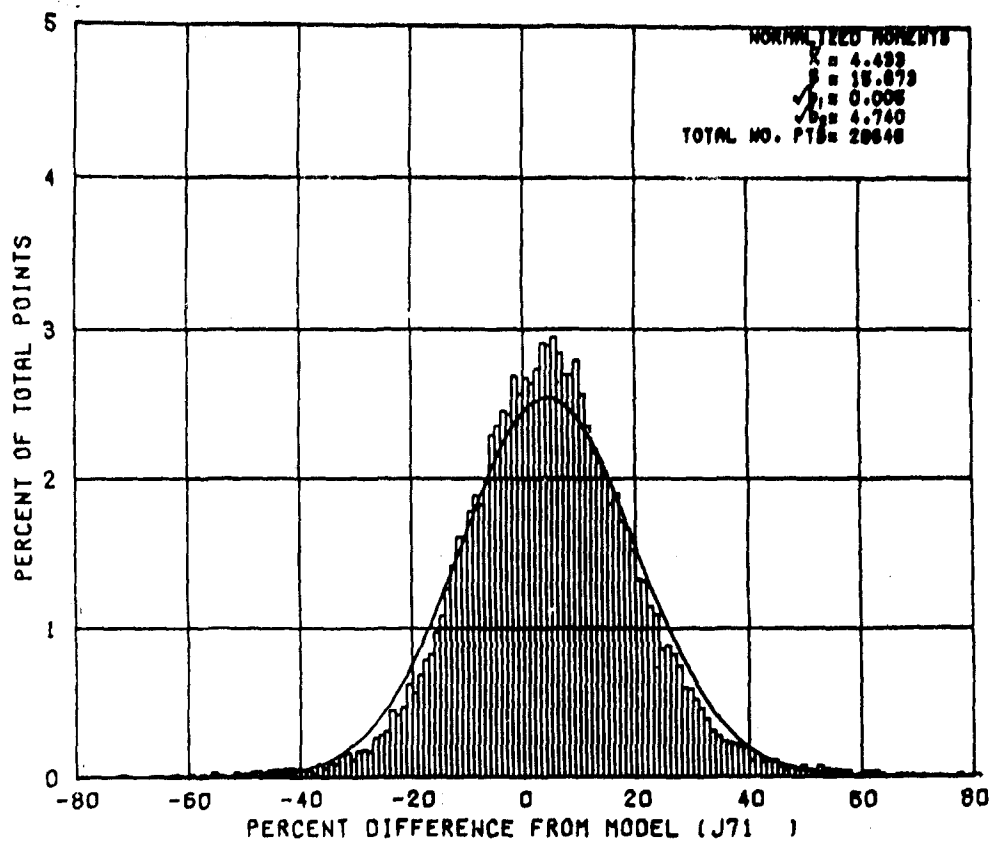


Figure 8b. Frequency Distribution of Percent Difference of AE-D Data From J71 Model

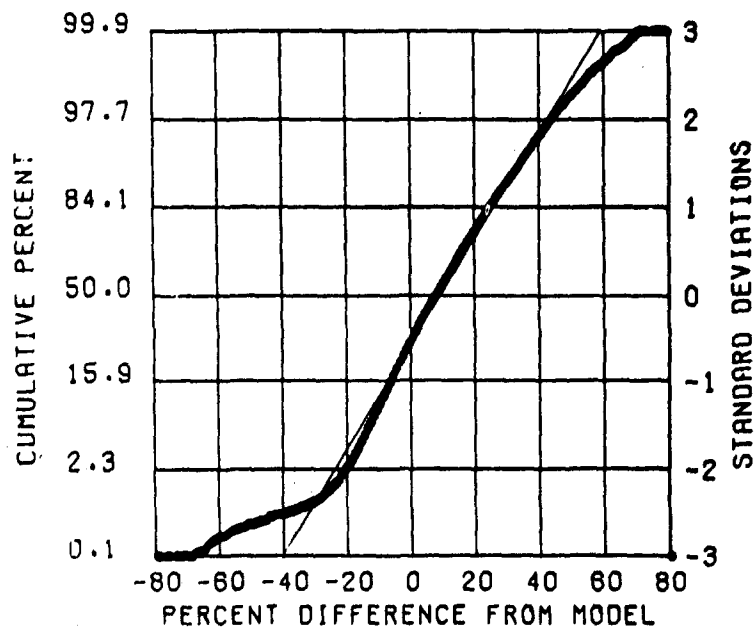


Figure 9a. Probability Distributions for AE-C Data Shown as Percent Departure From the J71 Model

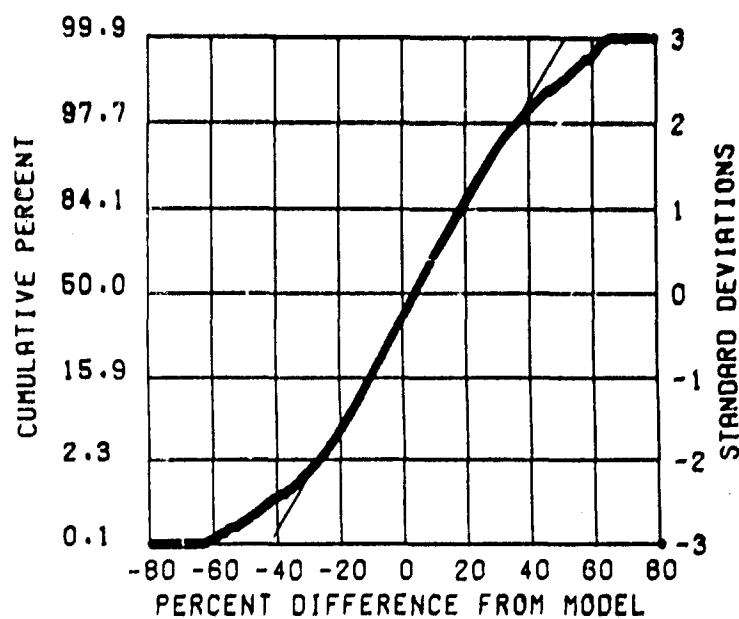


Figure 9b. Probability Distributions for AE-D
Data Shown as Percent Departure From the
J71 Model

Table 3. Modified Group I (AE-C, -D and -E) Total
Mass Density Ratio to Models (Altitude = 170-220 km;
Local Time = 08-24 hr; Kp Range = 0-9)

Model	Mean Ratio	Std Dev. (%)
1. MSIS 77	1.016	13.6
2. J73	1.033	13.8
3. J71	1.052	14.2
4. US66	0.892	15.2
5. J77	1.008	15.2
6. J64	0.890	15.3
7. J70	0.971	15.8
8. JWB	0.927	16.2
9. L-NASA	0.899	16.6
10. US62	0.717	24.7
11. DENSEL	1.233	28.3

Total No. of Points = 34,819

3.1.3 EFFECT OF DIGITAL FILTERING ON GROUP I DATA

Wave structures are presently not included in thermospheric models. Digital filtering tends to smooth the accelerometer data with a consequent underestimation of the variability. This factor has been examined by partitioning the Atmosphere Explorer results used for Table 4 into "spun" and "despun" orbits. These were obtained on an alternating schedule during the AE missions and thus provide comparable data sets as a function of flux, Kp, day, latitude, local time and altitude. Results are given in Table 4 using the J71, J77 and MSIS77 models. The despun data filtering results in about a 1.7 percent increase in the standard deviation compared to the spun data and a 0.8 percent increase compared to all data. It is believed that any wave structures not observed with the "10-15"-sec filter provide negligible contribution to the variability. Therefore, Tables 2 and 4 indicate that the best models reflect density variability for this data set with a standard deviation of about 15 percent.

Table 4. Comparison of Modified Group I (AE-C, -D and -E) Spun and Despun Mode Total Mass Density Ratio to Models (Altitude = 170-220 km; Local Time = 08-24 hr; Kp range = 0-9)

	All		Spun		Despun	
Model	Mean Ratio	Std Dev (%)	Mean Ratio	Std Dev (%)	Mean Ratio	Std Dev (%)
J71	1.052	14.2	1.040	13.3	1.063	15.0
J77	1.008	15.2	0.997	14.3	1.019	16.0
MSIS	1.016	13.6	1.004	12.6	1.030	14.4

No. of Points: 34,819 17,725 17,094

3.2 Group II Data Mean Ratios and Standard Deviations

Results of a statistical evaluation of the SETA-1, SETA-2, and S3-4 accelerometer measurements reduced with a "50-100"-sec filter are shown in Table 5. Listing of the models is in order of increasing average (unweighted) standard deviation for the three sets. The smallest standard deviation is associated with the unpublished J73 model, and varies from 7.70 to 10.34 percent. The latter value may be larger because of the preliminary state of processing needed to incorporate S3-4 data into this report. However, the standard deviations of 8-9 percent for SETA-1 and SETA-2 are typically 3-4 percent less than the results for the AE "spun" data

in Table 4. There are at least two reasons why smaller standard deviations would be expected from the Group II data. First, the "50-100"-sec filter smoothes out more of the atmospheric structure than the "30-77"-sec filter. For the AE data the difference between "spun" ("30-77" filter) and "despun" ("10-15" filter) data was 1.7 percent. A similar difference might be expected between the Group I and Group II data because of the additional range of wavelengths eliminated by the "50-100"-sec filter and the increase in occurrence and amplitude of longer period waves.¹¹ Second, the Group I data are for a mix of altitude, latitude and local time conditions, whereas for the Group II data, these conditions are highly correlated. For example, an analysis of AE-E data¹ showed that the standard deviation decreased by about 2 percent when the data were restricted to local times between 0800 and 0900 hours.

Table 5. Group II (SETA-1, SETA-2 and S3-4) Total Mass Density Ratio to Models (Altitude = 170-220 km; Local Time = 08-24 hr; Kp Range = 0-9)

Model	SETA-1		SETA-2		S3-4	
	Mean Ratio	Std Dev (%)	Mean Ratio	Std Dev (%)	Mean Ratio	Std Dev (%)
1. J73	0.916	9.03	0.942	7.70	0.934	10.34
2. J70	0.994	8.79	0.954	8.20	0.925	10.43
3. J71	0.935	9.10	0.983	8.07	0.974	10.68
4. MSIS77	0.974	10.20	0.969	8.02	0.970	11.30
5. US66	1.009	10.30	0.894	8.84	0.877	10.78
6. J64	1.010	10.41	0.889	8.85	0.870	10.71
7. MSIS79	0.973	10.51	0.969	8.32	0.968	11.65
8. JWB	0.913	9.84	0.829	9.07	0.827	12.17
9. J77	0.879	12.26	0.925	10.06	0.979	11.65
10. L-NASA	0.986	9.81	0.914	9.36	0.893	12.17
11. US62	1.158	11.17	0.973	12.12	0.927	16.97
12. DENSEL	0.890	14.32	0.938	11.44	0.770	17.74

No. of Points

42,835

32,950

36,953

11. Hines, C. O. (1974) The Upper Atmosphere in Motion, American Geophysical Union Monograph 18.

There are some differences in the relative accuracies of the models with respect to the three data sets of Table 5. The J71 model provides a better representation of density variations encountered by SETA-1 and S3-4 than does MSIS77. For the SETA-2 data, MSIS77 is slightly better than J71. The J77 model apparently is not an improvement over the other Jacchia models. It shows a standard deviation 2-3 percent greater than J71 and has an overall ranking of fourth from last for the three data sets. It is not recommended for operational applications.

Mean ratios in Table 5 are less than one for the most accurate models whereas the same models had mean ratios greater than one for the Group I data. Since the drag coefficients for both the Group I and Group II satellites are estimated to be within ± 10 percent,¹⁴ the difference cannot be unambiguously related to solar flux. The mean values for the first four models listed in Table 5 are 0.955 ± 0.029 , 0.962 ± 0.021 and 0.951 ± 0.025 for SETA-1, SETA-2 and S3-4, respectively. The variations are similar to those found for the Group I data. Interestingly, MSIS77 shows least change in mean value for the three Group II data sets. More extensive analyses, as accomplished in Reference 1, are planned for the larger data sets to be acquired. These studies will establish quantitatively the relationship between density and solar flux.

3.3 Data Partitioning Into Kp Bins

A further analysis of the J71, J77 and MSIS77 models has been carried out by partitioning the data into three Kp bins: Kp values 0 to 3, 3+ to 4+ and 5- to 9. This study involved the modified Group I data (Table 4) and the Group II data (Table 5).

3.3.1 GROUP I DATA

Table 6 shows results for the Group I data (Table 4) with spun and despun orbits considered separately. The differences between the standard deviations of the despun data and the spun data are larger for the 5- to 9 bin than for the 0 to 3 bin. These differences are about 0.5 percent, 1.1 percent and 0.5 percent for the J71, MSIS77 and J77 models, respectively. This difference is presumed due to additional wave structures associated with geomagnetic activity. The J71 and MSIS77 models show little variation of standard deviation with Kp. MSIS77 actually shows a slight decrease with increasing Kp, but the corresponding values of mean ratios show about a 10 percent increase. The indicated variability (standard deviation) is not representative of global conditions because the data base used for this study is weighted toward lower latitudes where geomagnetic storm effects are less significant. The only data poleward of 67° geographic latitude are provided by the short-lived AE-D mission. Further, the limited data in the high Kp bin are representative of only a few storms. Hence the altitudes, latitudes and local

times are more correlated than for data in the lower Kp bins. This tends to provide a standard deviation that is underestimated at high Kp bins relative to low Kp bins. Analysis of Group II data (Section 3.3.2) supports this hypothesis.

Table 6. Modified Group I (AE-C, -D and -E) Spun and Despun Mode; Total Mass Density Ratio to Models Partitioned Into Kp Bins (Altitude = 170-220 km; Local Time = 08-24 hr; 3 Kp Bins)

A. Model = J71						
	Spun			Despun		
Kp Range	No. Points	Mean Ratio	Std Dev (%)	No. Points	Mean Ratio	Std Dev (%)
All	17,725	1.040	13.32	17,094	1.063	14.98
0 to 3	11,688	1.044	13.23	11,118	1.063	14.77
3+ to 4+	4,360	1.032	13.66	4,222	1.058	15.51
5- to 9	1,877	1.034	12.97	1,754	1.076	14.96
B Model = MSIS77						
	Spun			Despun		
Kp Range	No. Points	Mean Ratio	Std Dev (%)	No. Points	Mean Ratio	Std Dev (%)
All	17,725	1.004	12.57	17,094	1.030	14.44
0 to 3	11,688	0.984	12.35	11,118	1.002	14.09
3+ to 4+	4,360	1.033	12.42	4,222	1.070	13.67
5- to 9	1,877	1.077	10.78	1,754	1.106	13.64
C. Model = J77						
	Spun			Despun		
Kp Range	No. Points	Mean Ratio	Std Dev (%)	No. Points	Mean Ratio	Std Dev (%)
All	17,725	0.997	14.32	17,094	1.019	16.01
0 to 3	11,688	0.997	13.66	11,118	1.015	15.12
3+ to 4+	4,360	0.997	15.12	4,222	1.018	17.15
5- to 9	1,877	0.997	16.32	1,754	1.042	18.15

3.3.2 GROUP II DATA

Table 7 shows results obtained by putting the Group II data into the same Kp bins. For the three data sets the increases in standard deviation from the 0 to 3 to 5- to 9 Kp bin range from 2.7-3.4 percent for J71, 4.1-5.5 percent for J77 and 0.7 to 5.6 percent for MSIS. Mean ratios generally decrease for J71 and J77 (typically 3-7 percent). This represents an increasing departure from unity, indicating that, on average, these models overestimate the observed geomagnetic response. MSIS77 shows a general increase in mean ratio except for the 3+ to 4+ to 5- to 9 bins for the S3-4 data. Results obtained from the more uniform latitudinal coverage of the Group II data show increased errors in the models during geomagnetically disturbed periods. However, the increases in these errors may be underestimated. Wave structure occurrences are known to increase during storm periods, and, as noted previously, the relatively heavy filtering of the Group II data means that part of the spectrum of the waves were not available for the analysis. (The filter was selected to permit convergence of an iteration technique to derive density and winds simultaneously from SETA data.) Hence, the Group I data may underestimate the standard deviations because of limited latitudinal distributions, whereas the Group II data underestimate the standard deviations because of data smoothing. A more comprehensive quantitative understanding of atmospheric variability during low solar flux conditions will require a more extensive set of global measurements. The effects of smoothing on the Group II data are further discussed in Section 3.5.

3.4 Data Partitioning in Kp, Latitude and Local Time Bins

More detailed analyses of the statistical properties of the accelerometer data have been made by further partitioning data into 10° geographic latitude bins and day/night local time bins as well as the three Kp bins used previously. Local time bins of 08-16 hr and 16-24 hr were used to separate Group II dayside and nightside northern hemisphere data occurring at the same latitude.

Mean values (relative to the J71 model) as a function of geographic latitude for the SETA-1, SETA-2 and S3-4 data are shown in Figure 10. Results are given here only for data obtained during low geomagnetic conditions ($Kp \leq 3$). The satellite altitudes as a function of latitude are similar for the data sets plotted. From right to left on the graph the altitude decreases from approximately 220 km at low northern hemisphere latitudes on the nightside to about 170 km near 30° N on the dayside. It then increases to about 220 km at midlatitudes in the southern hemisphere. All three data sets show a density bulge located around 60-70° latitude on the dayside. This implies that a localized high latitude density enhancement is a permanent feature of the dayside auroral region. The causative mechanism may be heating

related to the polar cusp. More detailed studies of this presently unmodelled source of density variability are being made. This result does emphasize that the combination of accelerometer capabilities and orbital characteristics provides a unique opportunity to obtain new fundamental information.

Table 7. Group II (SETA-1, SETA-2 and S3-4) Total Mass Density Ratio to Models Partitioned Into Kp Bins (Altitude = 170-220 km; Local Time = 08-24 hr; 3 Kp Bins)

Satellite = SETA-1 Satellite = SETA-2 Satellite = S3-4						
A. Model = J71						
Kp Range	Mean Ratio	Std Dev (%)	Mean Ratio	Std Dev (%)	Mean Ratio	Std Dev (%)
All	0.935	9.10	0.960	7.76	0.981	11.05
0 to 3	0.944	7.30	0.971	7.14	1.001	9.28
3+ to 4+	0.925	7.90	0.933	7.49	1.000	10.62
5- to 9	0.889	10.06	0.940	9.45	0.932	12.74
B. Model = MSIS77						
Kp Range	Mean Ratio	Std Dev (%)	Mean Ratio	Std Dev (%)	Mean Ratio	Std Dev (%)
All	0.974	10.20	0.969	8.02	0.970	11.30
0 to 3	0.971	9.76	0.960	7.59	0.982	9.22
3+ to 4+	0.968	10.53	0.990	7.90	1.013	12.25
5- to 9	1.008	10.49	0.990	9.06	0.940	14.82
C. Model = J77						
Kp Range	Mean Ratio	Std Dev (%)	Mean Ratio	Std Dev (%)	Mean Ratio	Std Dev (%)
All	0.879	12.26	0.938	10.06	0.979	11.65
0 to 3	0.893	11.55	0.939	8.62	0.984	8.97
3+ to 4+	0.868	12.89	0.908	11.45	1.012	11.82
5- to 9	0.847	15.63	0.875	12.62	0.944	14.46

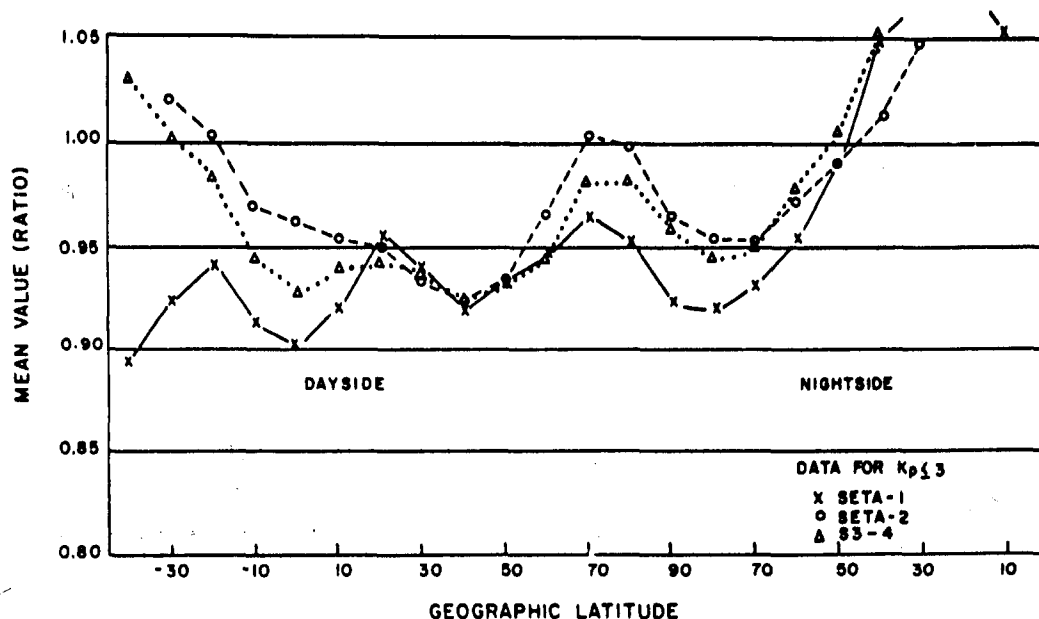


Figure 10. Mean Values of Ratios of SETA-1, SETA-2 and S3-4 Density Data to J71 Model Plotted as a Function of Geographic Latitude ($K_p \leq 3$)

Analysis of data obtained during low solar flux (Figure 7b) conditions showed that the J71 densities were underestimated near 200 km for local times around 2200 hr. This could be the cause of the observed mean density (ratio) increase with decreasing latitude on the nightside since the local time variations are less important at high latitudes. Further analyses of the SETA-2 and S3-4 data are required to determine whether the apparent ratio increase with latitude in the southern hemisphere is related to latitude, altitude or a systematic bias error related to the preliminary reduction state of these data sets.

Latitudinal changes of the standard deviations for the Group II data are shown for all three K_p bins in Figures 11a to 11c. These figures show that a maximum error in the models occurs near the pole, even during geomagnetically quiet conditions. The high-latitude standard deviations tend to increase with geomagnetic activity. Differences in the dependence on K_p for the three data sets are considered mainly a manifestation of the inadequacy of K_p as an indicator of geomagnetic activity. At lower latitudes the SETA-2 data indicate little variation of the standard deviation with K_p , whereas the SETA-1 and S3-4 results show an increase in standard deviation for the high K_p bin. However, analysis of the limited SETA-2 data reveals that SETA-2 did not encounter as large a range of geomagnetic conditions as SETA-1 and S3-4. Consequently, a more comprehensive study of the standard deviation vs latitude will be made using smaller K_p bins.

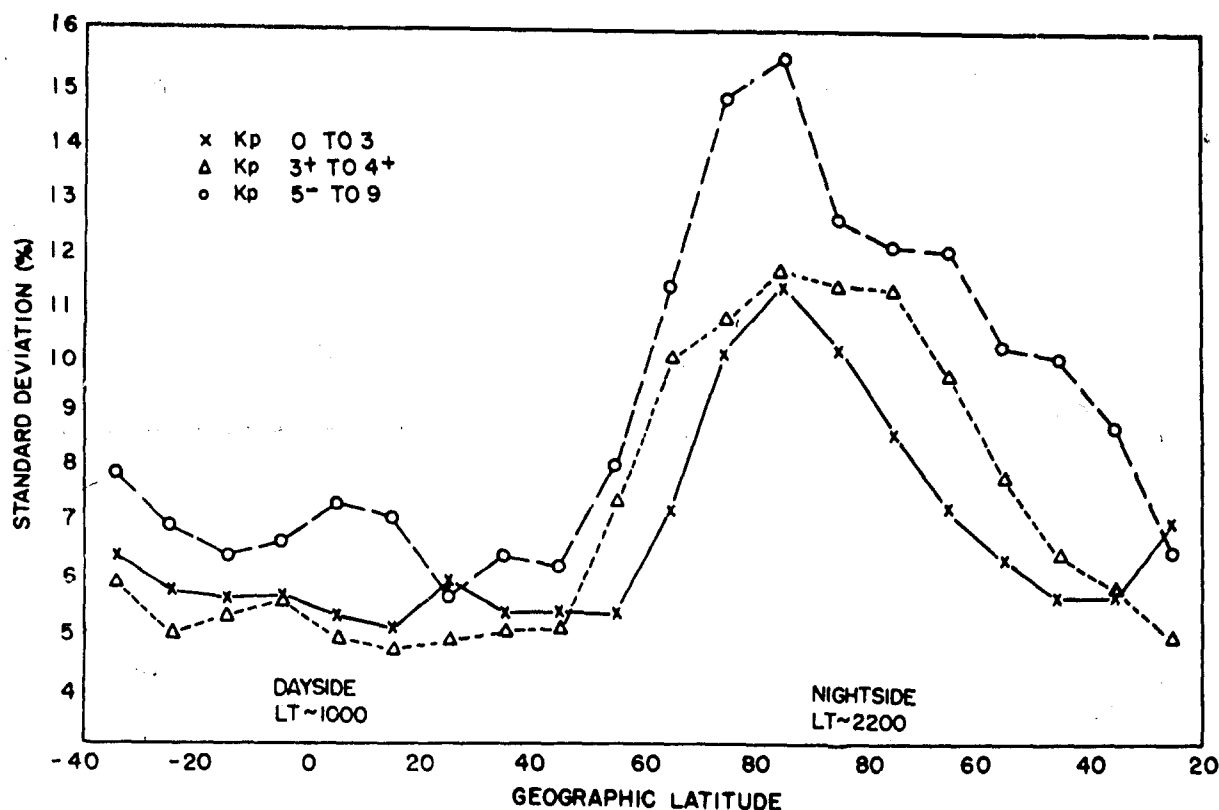


Figure 11a. Standard Deviations of Ratios of SETA-1 Density Data to J71 Model Plotted as a Function of Geographic Latitude

A similar analysis of standard deviation vs latitude for low solar flux conditions was made using S3-1 data. This satellite was selected because it had a sun-synchronous orbit and therefore provided good latitudinal coverage with little local time variation. Because of polar-crossings, two perigee local times ~ 22 hr and ~ 08 hr are mainly encountered at all latitudes. Figure 12 shows structured fluctuations in standard deviation that are apparently related to unmodelled density structures. In general, at high latitudes σ is greatest for the high Kp case. Lowest values, 8.5 ± 0.5 percent, occur between 10° N and 30° N. From 30 - 60° N, the standard deviation is roughly 11 ± 1.5 percent and from 30 - 60° S it is about 13 ± 3 percent. The lack of a more cohesive latitudinal structure for indicated variability is attributed to the mixing of altitude, latitude, day of year and local time.

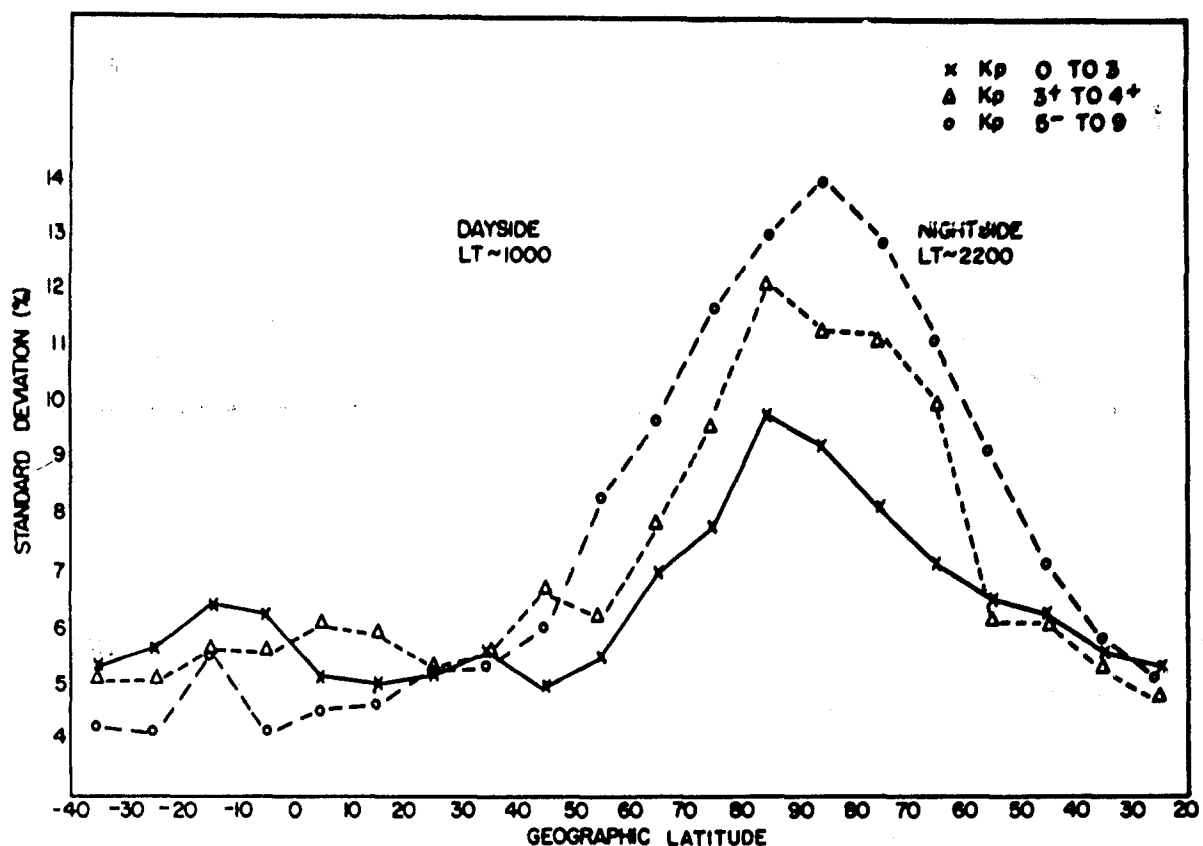


Figure 11b. Standard Deviations of Ratios of SETA-2 Density Data to J71 Model Plotted as a Function of Geographic Latitude

3.5 Effect of Digital Filtering on Group II Data

A quantitative description of the change in the standard deviation of Group II data due to latitude-dependent effects can be achieved if the data are filtered such that essentially all wave structures are passed through the filter. Preliminary processing techniques were developed in an attempt to reduce ten selected days of SETA-2 data with a "15-20"-sec filter. Five magnetically quiet days, one low activity day and four highly disturbed days were processed.

Figure 13 compares standard deviations vs latitude for three very quiet ($K_p < 1$) days, 22-24 May 82, using both the "15-20"-sec and "50-100"-sec filters. Results are given for the MSIS77 and J71 models. The "15-20"-sec filter gives standard deviations about 0.5 ± 0.5 percent greater than the "50-100"-sec filter. Some, possibly all, of this very small difference is attributable to additional vehicle dynamic accelerations passed by the "15-20"-sec filter. For latitude bins 30°N - 60°N on the nightside no data are plotted for the "15-20"-sec filter. This is because noise spikes, removed by the "50-100"-sec filter, were not rejected by the "15-20"-sec filter and produced large anomalies in the standard deviations. The

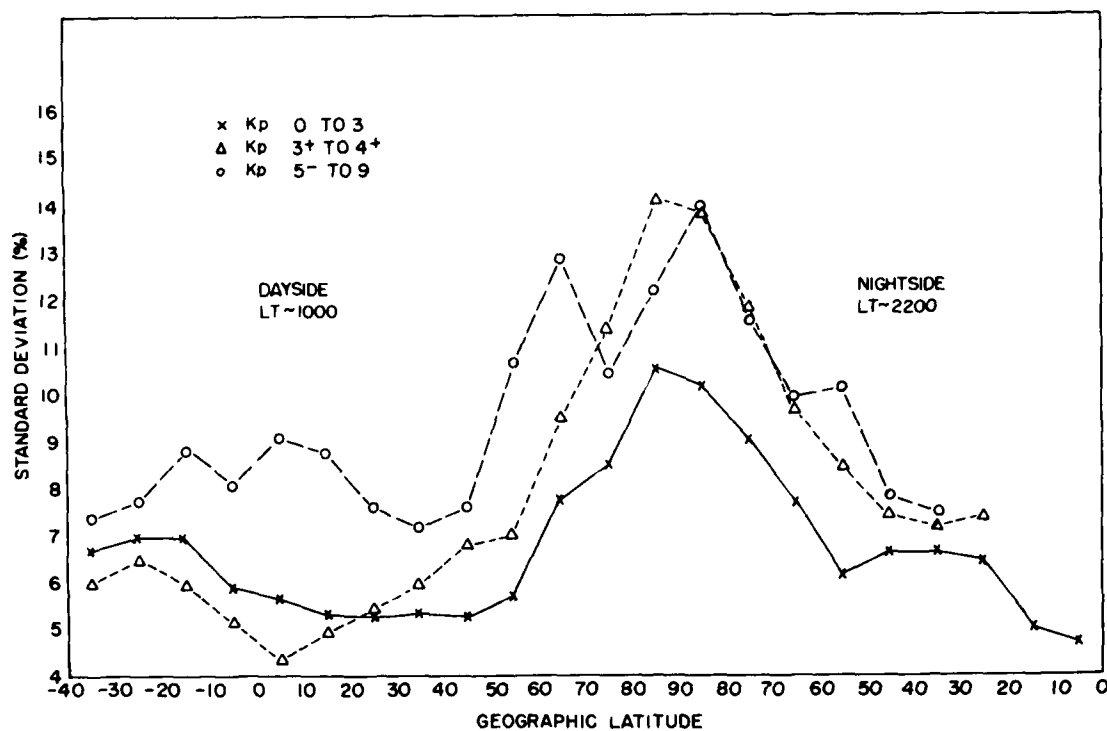


Figure 11c. Standard Deviations of Ratios of S3-4 Density Data to J71 Model Plotted as a Function of Geographic Latitude

present study indicates that, during extremely low geomagnetic conditions, wave structures with periods less than about 50 sec have very little effect on the standard deviation. Figure 13 is consistent with the results for the low Kp group of Figure 11, in that it shows the maximum standard deviation occurs at high latitudes. However, for the lower average geomagnetic conditions (Figure 13), the peak standard deviation is about 2 percent lower.

Results from three other periods studied with the "15-20"-sec filter are presented in Figure 14 in which the latitudinal distribution of the standard deviation is related to MSIS77. The data represent 12-hr periods each for low geomagnetic conditions on 10 July 82 ($\bar{K}p \sim 2^+$) and highly disturbed periods of 12 July 82 ($\bar{K}p \sim 5^+$) and 14 July 82 ($\bar{K}p \sim 7^+$). These results are considered tentative because of the difficulty in determining bias during storm periods without the availability of quiet-time data near these periods,⁴ and the need to obtain preliminary results on a short-term basis. Each curve is based on data from eight consecutive orbits. For 10 July 82, the standard deviation is less than 5 percent at latitudes below 50° N on the dayside. It reaches a peak of 14 percent near the pole. For 12 July 82 the

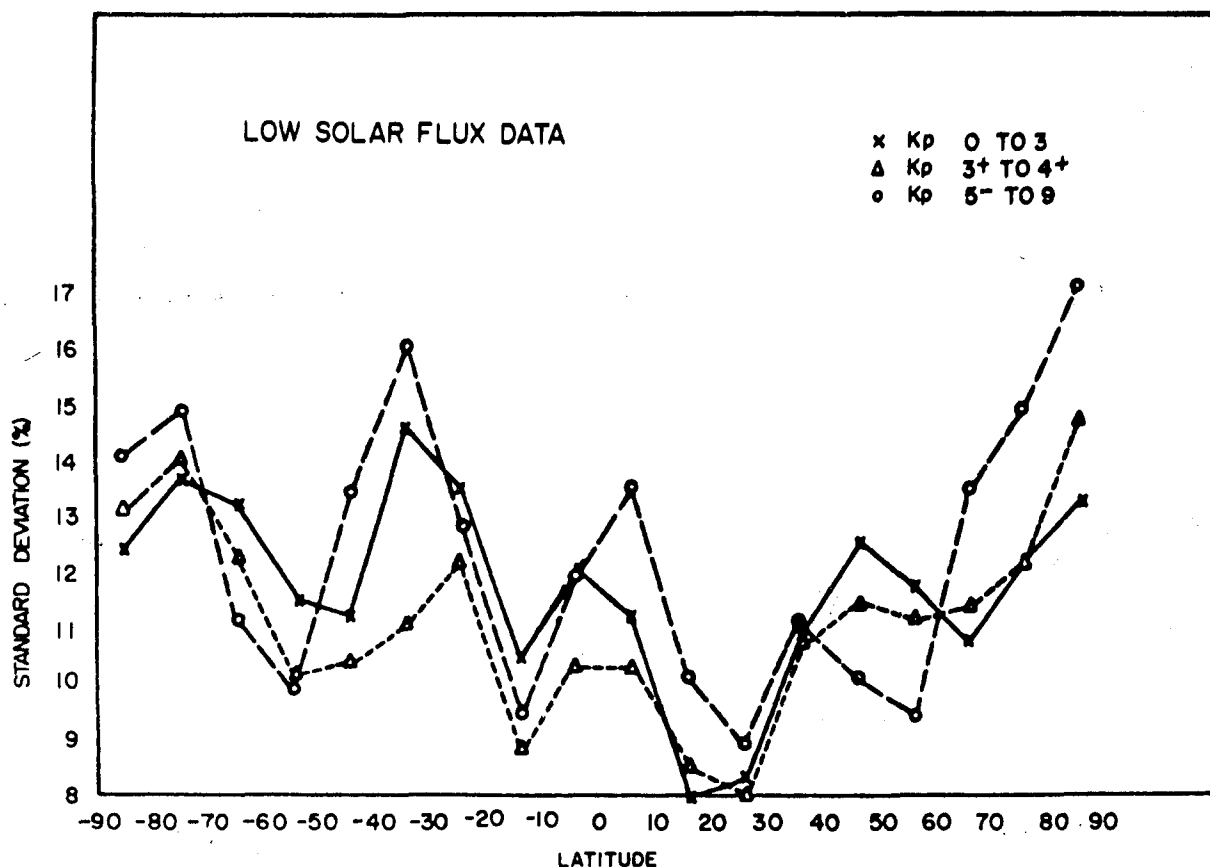


Figure 12. Standard Deviations of Ratios of S3-1 Density Data to J71 Model Plotted as a Function of Geographic Latitude

maximum standard deviation, 16 percent, is at 70-80° N on the dayside. The maximum for 14 July 82 is 19 percent and occurs in the nightside 90-80° latitude bin. The standard deviations exceed that of 10 July at all latitudes except below about 40° on the nightside. Although these results are preliminary, they indicate trends similar to those of Figure 11. The greater high latitude variations are assumed to be related to the extremely high level of geomagnetic activity. However, a much more extensive study of the recently acquired SETA-2 data and the required processing techniques using the "15-20"-sec filter, will be carried out. Such an effort would provide, for the first time, an accurate assessment of the influence of wave structures on density variability over the range of conditions encountered by the Group II data.

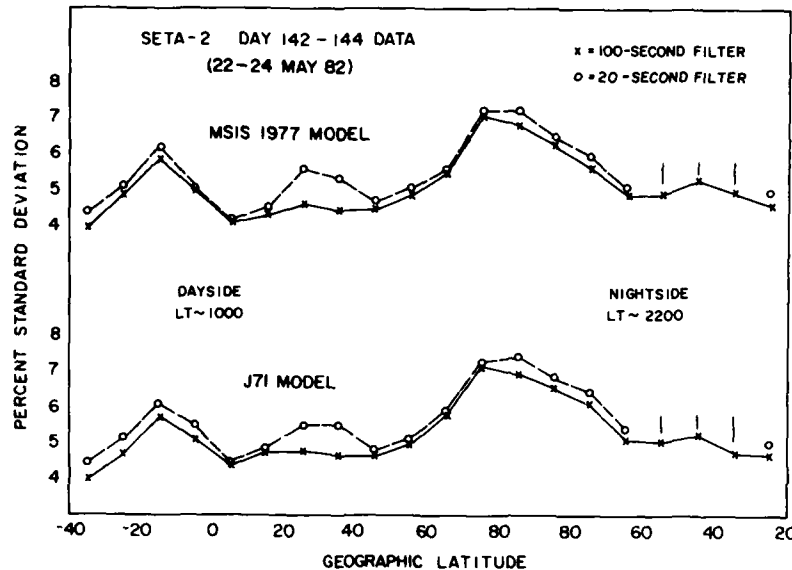


Figure 13. Effect of Digital Filter Bandwidth on SETA-2 Standard Deviations for (a) MSIS77 Model and (b) J71 Model for Quiet Geomagnetic Conditions

4. ATMOSPHERIC VARIABILITY

Results given in Section 3 show that the best models determine the average values of density and standard deviation (σ) to about ± 10 percent and ± 15 percent, respectively. Development of more accurate models will require significant improvements in our knowledge of the magnitude, distribution and transport of thermospheric heating. This section surveys the problems involved in obtaining the information and in relating it to density variability.

The complex phenomena contributing to atmospheric heating and dynamics are summarized in Figure 15. Solar EUV, the major thermospheric heat source, is deposited mainly at low latitudes in the summer hemisphere. The circulation and structure of the thermosphere at low and middle latitudes are controlled primarily by this heating. Upward propagating gravity waves and tides provide another energy source effective mainly at low and middle latitudes. At auroral latitudes electrodynamic coupling occurs between the magnetosphere, ionosphere and neutral atmosphere. Both the magnitude and spatial extent of the high-latitude heating are extremely variable and are related to the level of geomagnetic activity. Energetic charged-particle precipitation from the magnetosphere and Joule (resistance) heating due to electrical current systems within the ionosphere are important sources

of energy. These localized heat sources can cause large and sudden density variations, perturb circulation patterns and launch gravity waves. Also, ionospheric plasma, driven by the magnetospheric convection electric field, transfers momentum to the neutral particles and can produce strong winds. The wind systems induced by high latitude processes can significantly alter thermospheric density, composition and temperature on a global scale during disturbed geomagnetic conditions.

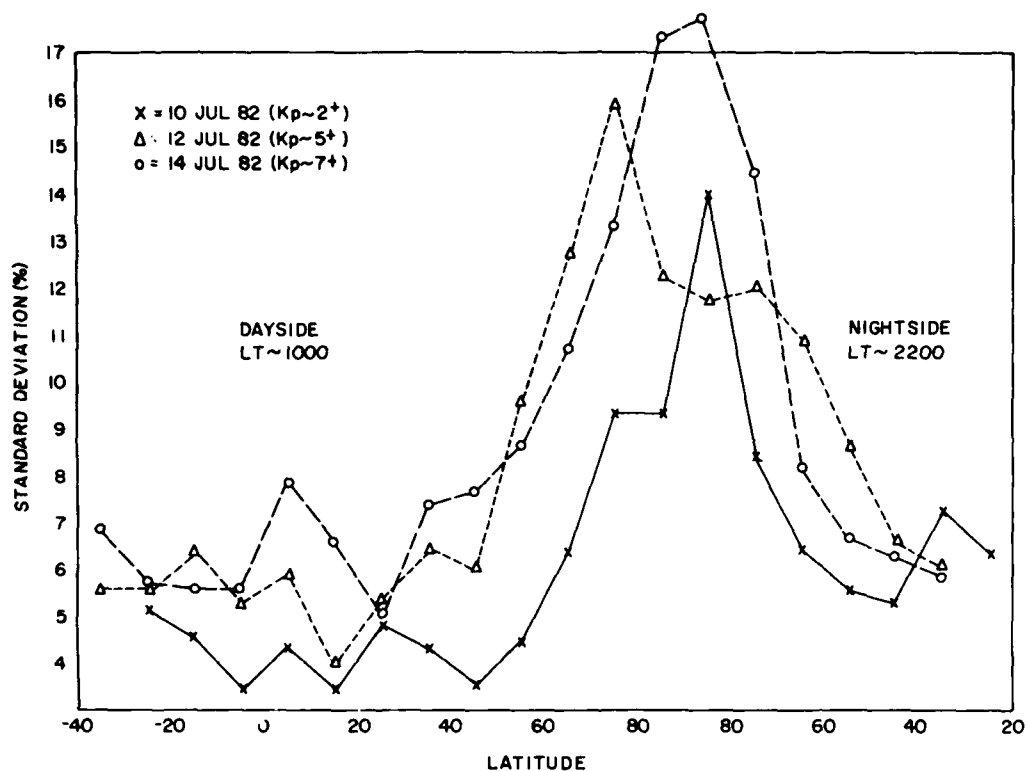


Figure 14. Standard Deviations of Ratios of SETA-2 Data to MSIS77 Model for Low, Moderate and High Geomagnetic Periods Plotted as a Function of Geographic Latitude

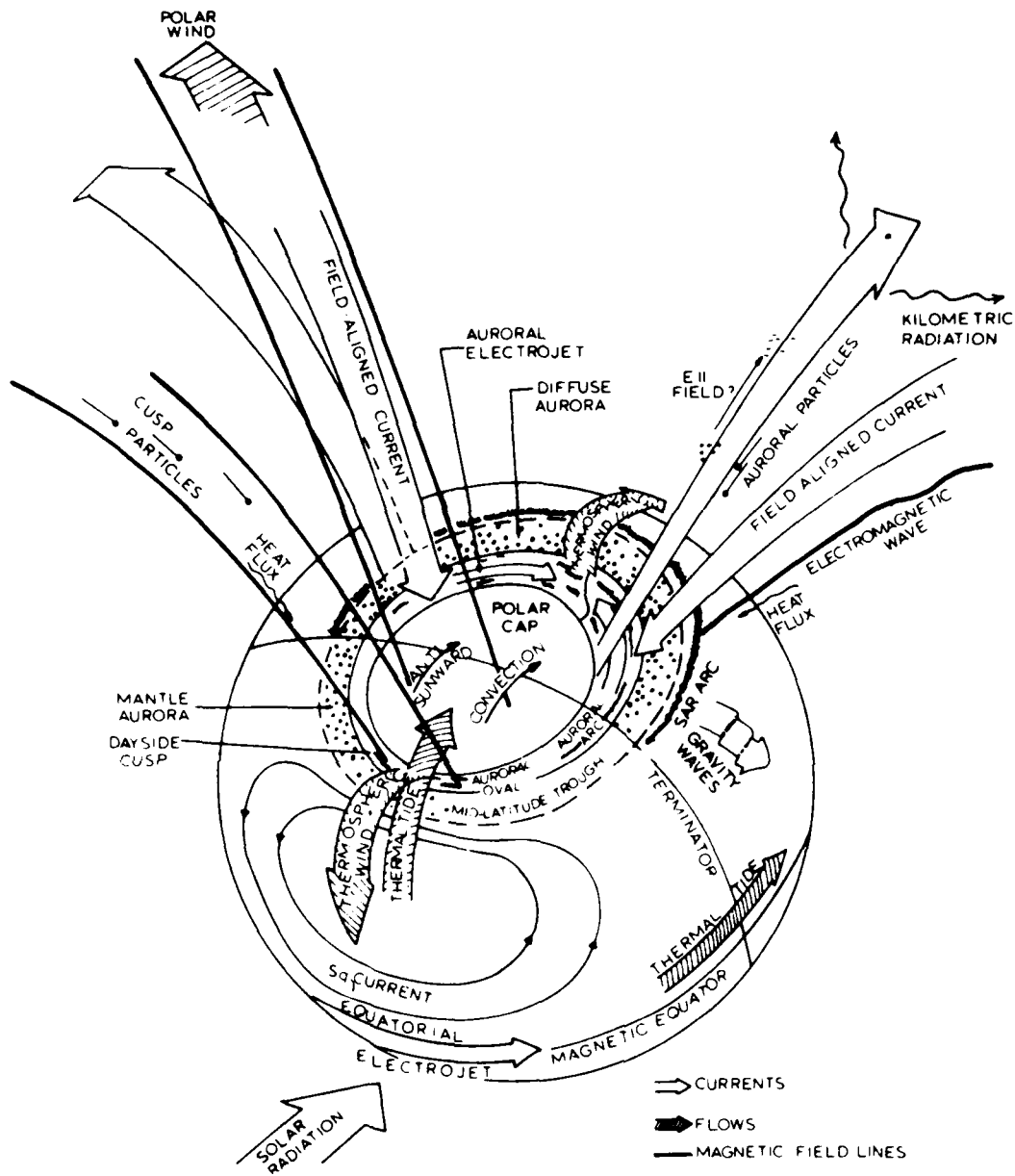


Figure 15. Schematic Representation of Heat Sources for the Upper Atmosphere

Density in the lower thermosphere is known to vary with the following parameters:

- (1) Solar flux (solar cycle and daily components)
- (2) Geomagnetic activity
- (3) Local time
- (4) Day of year
- (5) Latitude
- (6) Longitude
- (7) Wave structures.

Problems in achieving improved modelling of each of these factors are discussed below. However, it must be understood that the energetics, dynamics, chemistry, composition and resulting structure of the atmosphere are all functions of these factors and are so intricately related that it is not really possible to discuss each in isolation.

Solar Flux - The $F_{10.7}$ index used in all current models does not necessarily represent the complex mechanisms of interactions between the EUV flux and the thermosphere. Since it has been found to generally reflect variations in the thermospheric energy input, it is routinely used as a readily available, but imperfect, indicator of solar activity. It presents an additional problem for near real time operations. The solar-cycle dependent value of $F_{10.7}$ used in models is based on data some three months either side of the time of interest. Studies to determine the relationship between $F_{10.7}$ and satellite measurements of EUV are in progress.¹² An EUV reference spectrum for 1976-1981 has been developed. However, extrapolation outside this period is not recommended. Correlations have been found to be non-linear and both wavelength and solar-cycle dependent. In order to achieve the goal of ultimately utilizing direct measurements of the solar EUV flux in thermospheric models, an extensive measurement and data analysis program will be required. Methods of modelling UV irradiance based on detailed ground-based observations of the distribution of specific active regions across the solar-disk are also being investigated.¹³ Some promising results have been obtained but these studies are in preliminary stages.

Geomagnetic Activity - Large (up to ~100 percent) and short-term perturbations in neutral density and winds (~1 km/sec)^{5, 14} have been observed at high latitudes

-
12. Hinteregger, H. E. (1979) Development of Solar Cycle 21 Observed in EUV spectrum and atmospheric absorption, J. Geophys. Res. 84:1933.
 13. Oster, L., Schatten, K. H., and Sofia, S. (1982) Solar irradiance variations due to active regions, Astrophys. J. 256:768.
 14. Straus, J. M. (1978) Dynamics of the thermosphere at high latitudes, Rev. Geophys. Space Phys. 16:183.

in response to geomagnetic storms. Both the amplitude and phase of these fluctuations must be accurately modelled to significantly improve operational predictive capabilities. The problem is complicated because the storms are caused by high latitude heating processes that are not well understood and the density response depends on latitude, longitude, season, local time and solar cycle as well as storm intensity.

The planetary 3-hr Kp or ap index used as an indicator in most models does not necessarily represent the physical mechanisms responsible for density variations. However, it is the only routinely available index for geomagnetic activity. Based on a network of midlatitude stations, it is particularly limited when describing data at high latitudes.

Correlations of geomagnetic activity with the interplanetary magnetic field (B_1) magnitude and direction and the solar wind velocity (V) are being studied. Relations of the form $B_1^m V^n$ where $0.85 \leq m \leq 2$ and $1 \leq n \leq 2$ have been shown to provide a measure of energy transferred from the solar wind to the magnetosphere. These parameters also correlate highly with the auroral zone electrojet indices AE and AL.¹⁵ Eventually it may be possible to utilize an index derived from these solar wind and interplanetary magnetic field measurements as a precursor of geomagnetic activity. Considerable research to develop improved formulations relating any new index to the complicated density response would still be required.

The Dynamics Explorer¹⁶ satellites are monitoring relevant parameters involved in coupling between the magnetosphere, ionosphere and thermosphere. These measurements are being obtained at altitudes above 300 km. They provide direct inputs for evaluation and improvement of dynamic global circulation models¹⁷ and should lead to considerable progress in understanding the physics of geomagnetic storms. However, the resultant improvement to be realized in the specification of both the amplitude and phase of density variations due to a particular storm cannot be estimated at present. Also, the extrapolation of Dynamics Explorer data to altitudes below 200 km provides significant difficulties. There are few measurements of energetics and dynamics in this region to guide theoretical developments.

Local Time - The dominance of the semidiurnal tide below 200 km has recently been revealed by low-altitude satellite density measurements.^{18, 19, 20} At present, the referenced Jacchia models do not include this contribution to local time variations. Extensive theoretical progress has been made in describing both the diurnal and semidiurnal components as a function of altitude, latitude, season and solar flux.^{21, 22} In general, these results show good agreement with experimental data above 150 km. At lower altitudes significant day-to-day irregularities persist.

(Due to the large number of references cited above, they will not be listed here. See References, page 47.)

This is related to the interaction between local winds and tidal processes. These complicated dynamics make it difficult to establish the average tidal behavior. Over most of the region below 140 km the largest density perturbations generally occur at equatorial latitudes for the diurnal and semidiurnal tides. At 140 km the density uncertainty, depending on the phase of these two components, can be between 15 percent and 40 percent (J. M. Forbes, private communication).

Day of Year - Density variations with annual and sub-annual periodicities, as distinguished from periodic changes connected with the earth and sun, are a regular feature of the upper atmosphere. The "semi-annual variation" is generally characterized in current models by maxima near equinox and minima near solstice. At the present time, the cause of the semi-annual variation has not been unambiguously resolved. Ching and Chiu²³ have shown that EUV heating has the proper characteristics to be important at altitudes above 150 km. Mayr and Volland²⁴ have shown that sources in addition to EUV heating are required to account fully for this variation. High latitude heat sources, including auroral heating related to the semi-annual component of the occurrence of magnetic storms have been invoked. Walterscheid²⁵ recently has considered the semi-annual density variation as a conduction mode of oscillation essentially driven by Joule heating at high latitudes. This theoretical analysis shows good agreement with amplitude and phase vs altitude and latitude predicted by MSIS. Additional studies are needed to attain a more complete understanding of the semi-annual effect. MSIS (and other models) show a larger amplitude maximum in October than in April. Measurements using the satellite orbital decay technique²⁶ indicate that during low solar flux conditions the reverse is true.

Latitude - In addition to the latitude dependences associated with each of the above phenomena, present models also recognize seasonal-latitudinal variations. Jacchia⁷ has described contributions to this effect at thermospheric heights due to both the seasonal-latitudinal component of the diurnal temperature variation (strongly height dependent) and an intrinsic seasonal-latitudinal variation (not height dependent) with origin at the lower boundary of the thermosphere. In addition, below about 150 km, there is a variation due to the stratospheric and mesospheric seasonal variation which "spills over" into the lower thermosphere.

23. Ching, B. K., and Chiu, Y. T. (1972) Annual and sub-annual effects of EUV heating-I. Harmonic analysis, Planet. Space Sci. 20:1745.

24. Mayr, H. G., and Volland, H. (1972) Theoretical model for the latitude dependence of the annual and semiannual variations, J. Geophys. Res. 77:6774.

25. Walterscheid, R. L. (1982) Semiannual Oscillation in the Thermosphere as a Conduction Mode, Aerospace Corp. Rept. No. ATR-82 (9553) -1.

26. Walker, D. M. C. (1978) Variations in air density from January 1972 to April 1975 at heights near 200 km, Planet. Space Sci. 26:291.

Longitude - Satellite composition measurements have provided evidence of the influence of dynamics on longitudinal variations. Density maxima for heavy constituents occur at the longitude of the north and south magnetic poles. The behavior of the lighter constituents is negatively correlated. This behavior is related to plasma density and motion influenced by earth's magnetic field. Ion-neutral coupling is therefore involved in determining the longitudinal distribution of the neutral density. The MSIS 1979⁹ model included terms dependent upon geographic latitude, longitude, universal time, solar flux and geomagnetic activity to account for this variation. However, the standard deviation of the data shown in Table 5 was about 0.3 percent higher with this model than with the MSIS 1979 model which was longitudinally averaged, indicating the difficulty in modelling this variation.

Waves - Large-scale gravity waves having periods different from those of tidal waves and not directly related to the earth-sun-moon geometry, also occur in the atmosphere. These may be generated either locally in the thermosphere or at lower altitudes. Gravity waves with the largest amplitudes observed at high latitudes were detected by the accelerometers on the OV1-15 satellite.²⁷ These were related to the intensity of high-latitude heating as indicated by the auroral electrojet index. The Kp index was found to be a poor indicator of wave generation.²⁸ Evidence of wave structure with location dependent on earth's tropospheric weather patterns has been found in the analysis of Atmosphere Explorer ion gauge data.²⁹ A comprehensive survey of wave structures in neutral constituents was made using 338 orbits of data from the open-source neutral-mass spectrometer on AE-C.³⁰ The highest wave amplitudes (up to 55 percent peak-to-peak) and greatest number of occurrences were in both the northern and southern high-latitude regions. These were associated with a high-latitude conjugate phenomenon such as Joule heating and/or particle precipitation. At $\pm 25^\circ$ magnetic latitude, secondary maxima in low amplitude waves (5-15 percent) were attributed to a near equatorial source.

These wave phenomena are not incorporated into present models. While some of the features of wave structures associated with geomagnetic activity are becoming known, a capability for accurately predicting such behavior may not be possible in the foreseeable future. Also, planetary and gravity waves with sources in the troposphere or stratosphere appear to propagate into the thermosphere and dissipate

27. Marcos, F.A., and Champion, K.S.W. (1972) Gravity waves observed in high latitude neutral density profiles, Space Res. 12:791.
28. Forbes, J.M., and Marcos, F.A. (1973) Thermospheric density variations associated with auroral electrojet activity, J. Geophys. Res. 78:3841.
29. Rice, C.J., and Sharp, L.R. (1977) Neutral atmospheric waves in the thermosphere and tropospheric weather systems, Geophys. Res. Lett. 4:315a.
30. Potter, W.E., Kayser, D.C., and Mauersberger, K. (1978) Direct measurements of neutral wave characteristics in the thermosphere, J. Geophys. Res. 81:5002.

energy by viscous interactions. Their influence on heating and transport must be investigated.

Table 8 summarizes the approximate magnitude and time scale for density increases associated with each of the above phenomena. Results are given for an altitude of 200 km. Magnitudes are representative of those in current models except for the wave value, which is based on measured data.

Table 8. Thermospheric Density Variability at 200 km

Effect	$\Delta\rho$ 200 km	Time Scale
1. Flux (Solar Cycle)	100%	Years
2. Flux (Daily)	10%	Day
3. Geomagnetic Activity	100%	Hours
4. Local Time	15%	Hours
5. Semi-Annual	40%	Months
6. Latitude	25%	Months
7. Longitude	5%	Day
8. Waves	50%	Minutes

5. RECOMMENDATIONS

Sections 3 and 4 have shown that the existing need for very accurate knowledge of both absolute density and its variability require a long-term program involving:

(a) More realistic indices to describe energy inputs related to solar EUV and auroral processes.

(b) An extensive measurements program to provide a basis for developing accurate relationships between energy inputs and density variability.

(c) Development of accurate dynamic global circulation models that can better determine how the thermosphere is affected by internal and external influences.

Many of the efforts directed toward replacing $F_{10.7}$ and K_p were discussed at the Satellite Drag Workshop.³¹ It was concluded that more realistic solar and geomagnetic indicators are still at least several years away. Until better indices become available, there will be a fundamental limitation on model accuracies.

31. Space Environment Services Center (1982) Proceedings of a Workshop on Satellite Drag, March 18-19, 1982, U.S. Dept. of Commerce, Boulder, Colorado.

There remains a critical need for data at all altitudes in the lower thermosphere. The problem is particularly acute at high latitudes and below 150 km. Atmosphere Explorer data were obtained mainly above 150 km. Also, AE-D, the polar orbit mission, lasted only a few months due to a spacecraft power failure. The Space Science Board³² has pointed out the importance of determining the mean circulation and temperature structure as well as changes in the tidal structure and changes in geomagnetic activity to understand the region below 150 km.

Global circulation models are being continually updated and improved. A recent revision includes the incorporation of the effects of the high-latitude convection electric field.³³ Dynamics Explorer data will permit significant advances in magnetic disturbance morphology at altitudes above 300 km. However, it should be at least another 5-10 years before these dynamic models can achieve the accuracies of present empirical models. Additional extensive effort beyond this time frame will be needed to extend these models accurately at altitudes below 200 km and to demonstrate better accuracy than empirical models.

It appears that, at least through this decade, there will not be an alternative to direct measurements for knowledge of absolute density and its variations. Remote sensing techniques for global monitoring are being investigated, but even if implemented successfully, they may not achieve the required accuracies. Eventually, as models and, possibly, remote sensing techniques improve, directly measured data may be needed only for normalization, updating and fine-tuning of model predictions.

The remainder of this section deals with three requirements to improve understanding of absolute density and its variability: first, a technique to provide required-accuracy density measurements using the satellite accelerometer experiment; second, utilizing this technique an extensive measurements program to provide the basis for development of more accurate models; and third, other needed supporting efforts.

5.1 Absolute Density Determination

An improved method of determining absolute density can be obtained by exploiting accelerometer capability to provide extremely accurate drag measurements. Density is extracted from the drag data by the relation:

32. Committee on Solar-Terrestrial Research (1981) Solar-Terrestrial Research for the 1980's, National Academy Press, Washington, D. C.

33. Roble, R. G., Dickinson, R. E., and Ridley, E. C. (1982) Global circulation and temperature structure of thermosphere with high latitude plasma convection, J. Geophys. Res. **87**:1599.

$$\rho = \frac{2 M a_D}{A C_D V^2 \cos \theta} \quad (3)$$

where ρ is density, a_D is the measured drag acceleration, θ is the angle between the accelerometer and drag vector and M , A , C_D and V are, respectively, the satellite's mass, cross sectional area, drag coefficient and the atmospheric mass velocity (relative to the satellite). The required experiment, which could routinely measure absolute density to about ± 5 percent, should have the following characteristics:

- (1) A spherical shape for accurate area determination and improved theoretical drag coefficient estimate.
- (2) An elliptical orbit to permit calculation of accelerometer noise and bias near apogee.
- (3) An accurate attitude system to reduce errors in θ .
- (4) A minimum of extraneous accelerations due to vehicle dynamics.
- (5) A lifetime of several months in a relatively low orbit (below 150 km) to acquire data over a wide range of variables.
- (6) Incorporation of a wind sensor to reduce errors in determining the atmospheric velocity relative to the satellite.
- (7) Incorporation of a calorimeter experiment to further improve drag coefficient estimates (A. Prag, private communication).

A mass spectrometer should also be a part of the above experiment. Although it may not provide as accurate total density data as the accelerometer experiment, the composition data are invaluable for interpreting variations in density. These experiments also complement each other since the accelerometer can provide vertical and cross-track winds and the mass spectrometer can provide along-track winds.

5.2 Measurements Programs

The satellite accelerometer experiment is crucial for advancing our knowledge of density and its variability in the lower thermosphere. To date it has provided the only comprehensive set of measurements during high solar flux conditions as well as an extensive low solar flux data base. As shown in Sections 3 and 4, additional extensive measurements are needed to permit continued improvements in operational capabilities. Also, the Space Science Board³² has stressed the need for continued spacecraft investigations of the upper atmosphere throughout the 1980's to ensure adequate geographic, local time, seasonal and solar-cycle coverage.

The first set of measurements suggested is an extension of the Group II data set to lower solar flux conditions as follows:

(1) An accelerometer flown during 1983 has provided data during intermediate solar flux conditions. These data must be incorporated into the density data base and analyzed.

(2) An opportunity exists to fly an accelerometer on a host vehicle during 1985. A partially fabricated instrument could be completed in time to meet the flight schedule. Correlative measurements, particularly a mass spectrometer, should also be flown on this mission. Other desired payloads include a wind sensor and a calorimeter. This mission would provide data near solar minimum and would furnish systematic measurements of high-latitude dynamic processes that were not obtained with AE-D.

These two flights, combined with the Group II data, would provide a consistent data set to improve formulations of density variability as a function of solar flux, geomagnetic activity, day of year, longitude and wave structures as a function of latitude above 170 km. This program should be extended, using the payload suggested for item 2 above, with heat source measurements, to obtain year-round data in the northern hemisphere in (1) a noon-midnight orbit and (2) a dawn-dusk orbit. These missions should overlap by a few months to permit more detailed analysis of local time variations and geomagnetic storm-related density and circulation variations.

The next set of measurements should provide an expanded study of the dynamics of the lower thermosphere. The absolute density experiment of Section 5.1 with composition and wind data should routinely explore density structure at altitudes as low as 130 km. A pair of simultaneous satellites with lifetimes greater than one year is suggested. The spacecraft would consist of a low- and a high-inclination mission. The concept is similar to the overlapping AE-D and AE-E missions concept which was carried out for only a short time. The objective would be to provide accurate density data at critical lower altitudes. Such missions will require trade-offs between available propulsion capability, perigee and apogee heights and experiment operations. Follow-on missions are needed for solar-cycle coverage. These missions should also be coordinated with other onboard experiments or satellite and ground-based experiments that monitor solar energy inputs, ionospheric plasma, electric fields and charged particle precipitation. Tethered satellite missions should also be considered, when available.

5.3 Supporting Studies

Other efforts that can lead to an improved capability to specify the density at satellite altitudes include the following:

(1) Below about 250 km there is very little data on atmospheric dynamics. Detailed studies of the morphology of density and wind during storm periods encountered by SETA-1 are being carried out. These studies will also incorporate temperatures derived from incoherent scatter radar data. The above efforts form the basis for development of the required more extensive analyses. These analysis efforts involving valuable data in regions of particular interest should be continued with the more recent data sets.

(2) New indices for solar and geomagnetic activity should be tested, when available, using the present Group I and Group II accelerometer data sets (assuming the indices are based on data available during the time periods of the density measurements).

(3) Both empirical and dynamic models should be improved using results from above analyses.

(4) The feasibility of using auroral imaging techniques or heating measurements to relate auroral zone heating to density variability should be investigated. In particular, it should be determined whether regions of intense heating can be related to wave generation.

6. CONCLUSIONS

Satellite density measurements using accelerometers have provided an extensive description of the variability of the neutral atmosphere. Mean densities are believed to be given within ± 10 percent by the most accurate models. This uncertainty can be reduced to about ± 5 percent by an accelerometer experiment such as described in Section 5.1. Low solar flux results derived from AE-C, -D and -E and S3-1 satellites indicate that the best models have a standard deviation of about ± 15 percent. For the higher solar flux data from SETA-1, SETA-2 and S3-4 the standard deviation was near 9 percent. This lower value is attributed to the additional smoothing due to the 50-100 sec filter and the high correlation of altitude, latitude and local time for this data set. The measurements did show an increased model uncertainty at high latitudes.

The following efforts can be easily accommodated into existing programs and provide important results needed to augment and define future activities:

(1) A consistent set of data with excellent solar-cycle coverage can be achieved by a 1985 flight of an accelerometer on a host vehicle. The results would extend the present Group II data base to low solar flux conditions and provide a unique basis for evaluation and improvement of density models.

(2) Density and wind measurements from the SETA-1 and -2 experiments already provide a unique opportunity to obtain fundamental new results. Data analysis efforts are being made to understand the dynamic processes influencing density variability. Such studies will lead to improved modelling of density in the thermosphere. Additional data analysis support would produce these results on a timely basis.

The accuracy that models can ultimately achieve cannot be specified at present. Further, sufficient data are not yet available to fully assess present model errors. The problems involved in improving models and an indication of some of the on-going efforts directed toward their resolution were summarized in Section 4. Major problem areas are wave structures and high-latitude processes involved during geomagnetic storms. Significant reductions in density uncertainties appear to be achievable but require long-term programs involving synoptic measurements coordinated with theoretical studies and modelling efforts.

References

1. Marcos, F.A., McInerney, R.E., and Fioretti, R.W. (1978) Variability of the Lower Thermosphere Determined From Satellite Accelerometer Data, AFGL-TR-78-0123, AD A058982.
2. Marcos, F.A., Gillette, D.F., and Robinson, E.C. (1982) A Global Thermospheric Density Model Based on Satellite Accelerometer Data, AFGL-TR-82-0025, AD A119861.
3. Marcos, F.A., and Champion, K.S.W. (1979) Satellite Density Measurements With a Rotatable Calibration Accelerometer (ROCA), AFGL-TR-79-0005, AD A069740.
4. Marcos, F.A., and Swift, E.R. (1982) Application of the Satellite Triaxial Accelerometer to Atmospheric Density and Wind Studies, AFGL-TR-82-0091, AD A120852.
5. Champion, K.S.W., and Marcos, F.A. (1973) The triaxial accelerometer system on Atmosphere Explorer, Radio Sci. 8:197.
6. Bramson, A.S., and Slowey, J.W. (1974) Some Recent Innovations in Atmospheric Density Programs, IBM Corp., AFCRL-TR-74-0370, AD 786414.
7. Jacchia, L.G. (1977) Thermospheric Temperature Density and Composition: New Models, Special Rept. 375, Smithsonian Astrophys. Observatory, Cambridge, Massachusetts.
8. Hedin, A.E., Salah, J.E., Evans, J.V., Reber, C.A., Newton, G.P., Spencer, N.W., Kayser, D.C., Alcayde, D., Bauer, P., Cogger, L., and McClure, J.P. (1977) A global thermospheric model based on mass spectrometer and incoherent scatter data, MSIS 1, N_2 density and temperature, J. Geophys. Res. 82:2139.
9. Hedin, A.E., Reber, C.A., Spencer, N.W., and Brinton, H.C. (1979) Global Model of longitude/UT variations in thermospheric composition and temperature based on mass spectrometer data, J. Geophys. Res. 84:1.

References

10. Noonan, J. P., Fioretti, R. W., and Hass, B. (1975) Digital Filtering Analysis Applied to the Atmosphere Explorer-C Satellite MESA Accelerometer Data, AFCRL-TR-75-0293, AD A015765.
11. Hines, C. O. (1974) The Upper Atmosphere in Motion, American Geophysical Union Monograph, 18.
12. Hinteregger, H. E. (1979) Development of Solar Cycle 21 Observed in EUV Spectrum and Atmospheric Absorption, J. Geophys. Res. 84:1933.
13. Oster, L., Schatten, K. H., and Sofia, S. (1982) Solar irradiance variations due to active regions, Astrophys. J. 256:768.
14. Straus, J. M. (1978) Dynamics of the thermosphere at high latitudes, Rev. Geophys. Space Phys. 16:183.
15. Holzer, R. E., and Slavin, J. A. (1982) A quantitative model of geomagnetic activity, J. Geophys. Res. 87:9054.
16. Hoffman, R. A., and Schmerling, E. R. (1981) Dynamics explorer program: an overview, Space Sci. Instr. 5:345.
17. Dickinson, R. E., Ridley, E. C., and Roble, R. G. (1981) A three-dimensional general circulation model of the thermosphere, J. Geophys. Res. 86:1499.
18. Sharp, L. R., Hickman, D. R., Rice, C. J., and Straus, J. M. (1978) The altitude dependence of the local time variation of thermospheric density, Geophys. Res. Lett. 5:261.
19. Forbes, J. M., and Marcos, F. A. (1979) Tidal variations in total mass density as derived from the AE-E MESA experiment, J. Geophys. Res. 84:31.
20. Forbes, J. M., and Marcos, F. A. (1980) Seasonal-latitudinal tidal structures of O, N₂, and total mass density the thermosphere, J. Geophys. Res. 85:3489.
21. Forbes, J. M. (1982) Atmospheric tides, 1. Model description and results for the solar diurnal component, J. Geophys. Res. 87:5222.
22. Forbes, J. M. (1982) Atmospheric tides, 2. The solar and lunar semidiurnal components, J. Geophys. Res. 87:5241.
23. Ching, B. K., and Chiu, Y. T. (1972) Annual and sub-annual effects of EUV heating-I. Harmonic analysis, Planet. Space Sci. 20:1745.
24. Mayr, H. G., and Volland, H. (1972) Theoretical model for the latitude dependence of the annual and semiannual variations, J. Geophys. Res. 77:6774.
25. Walterscheid, R. L. (1982) Semiannual Oscillation in the Thermosphere as a Conduction Mode, Aerospace Corp. Rept. No. ATR-82-(9553)-1.
26. Walker, D. M. C. (1978) Variations in air density from January 1972 to April 1975 at heights near 200 km, Planet. Space Sci. 26:291.
27. Marcos, F. A., and Champion, K. S. W. (1972) Gravity waves observed in high latitude neutral density profiles, Space. Res. 12:791.
28. Forbes, J. M., and Marcos, F. A. (1973) Thermospheric density variations associated with auroral electrojet activity, J. Geophys. Res. 78:3841.
29. Rice, C. J. and Sharp, L. R. (1977) Neutral atmospheric waves in the thermosphere and tropospheric weather systems, Geophys. Res. Lett. 4:315a.
30. Potter, W. E., Kayser, D. C., and Mauersberger, K. (1978) Direct measurements of neutral wave characteristics in the thermosphere. J. Geophys. Res. 81:5002.

References

31. Space Environment Services Center (1982), Proceedings of a Workshop on Satellite Drag, March 18-19, 1982, U.S. Dept. of Commerce, Boulder, Colorado.
32. Committee on Solar-Terrestrial Research (1981) Solar-Terrestrial Research for the 1980's, National Academy Press, Washington, D.C.
33. Roble, R.G., Dickinson, R.E., and Ridley, E.C. (1982) Global circulation and temperature structure of thermosphere with high-latitude plasma convection, J. Geophys. Res. 87:1599.